Contents

CHAPTER 1

The Constituents of the Nucleon

1.1 INWARD BOUND

Scattering experiments have played a decisive role in unravelling the structure of matter. A fascinating account of our understanding of matter and forces in the physical world is given by Pais[1] in his book "Inward Bound". Pais recounts the recorded reaction of Rutherford to the observation of back-scattering[2] of α-particles (about 1 in 8000) by a thin gold-foil: "It was quite the most incredible event that has ever happened to me in my life. It was almost as incredible as if you fired a 15-inch shell at a piece of tissue paper and it came back and hit you". That was when the atomic nucleus was discovered. Sixty years later, history repeated itself when a SLAC-M.I.T. team of scientists performed[3] inelastic electron-proton scattering with incident electron energies between 7 and 17 GeV at the Stanford linear accelerator. In the reaction $e + P \to e' + X$, they only counted the number of outgoing electrons e' at 6° and 10° angles, leaving the debris X unobserved. Such cross-sections are termed "inclusive". To their surprise, the experimenters observed hundreds of times more counts at these angles than expected. In elastic scattering $e + P \to e' + P'$, the outgoing particles are the same as the incoming ones, and the cross-section falls-off very fast as a function of the scattering angle due to the finite size of the nucleon. The orginal experimental result, shown in Fig. 1.1, indicated that in high-energy inelastic scattering, the incoming electrons occasionally hit hard point-like constituents inside the proton, just as in Rutherford's experiment the incident α-particle was sometimes scattered

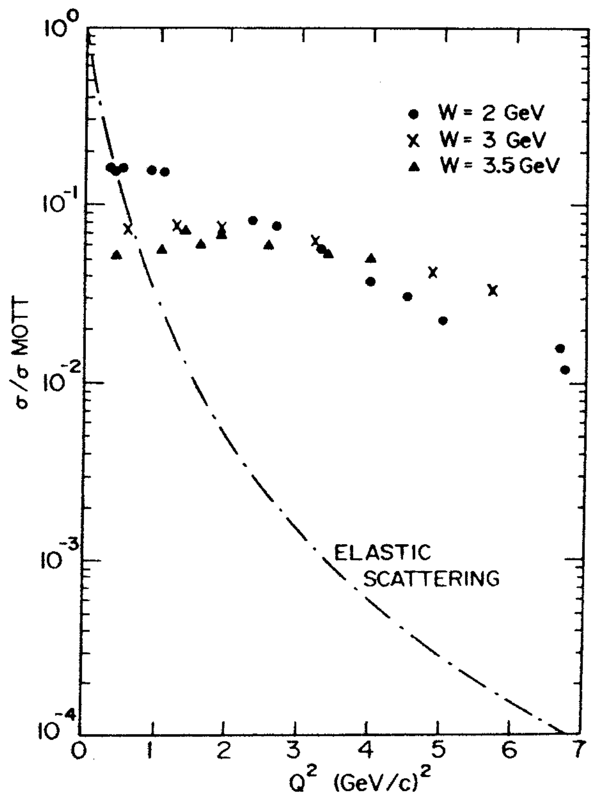

Figure 1.1 Deep inelastic electron-proton scattering (Ref. 3). The double differential inclusive cross section, divided by the Mott cross section for elastic scattering from point particles, $(d^2\sigma/d\Omega dE')/\sigma_{\mathrm{Mott}}$, is plotted as a function of the four-momentum squared, Q^2. The process is depicted in Fig. 1.2 . Note that $Q^2 = 2EE'(1 - \cos\theta)$, where E, E' are the energies of the incident and scattered electron, and θ is the scattering angle. The data are shown for various values of the invariant mass of the recoiling target system, W, and compared with the elastic cross section which falls off much more rapidly. See text for more details.

ental result, shown in Fig. 1.1,
ıttering, the incoming electrons
ıt side the proton, just as in
ar. e was sometimes scattered

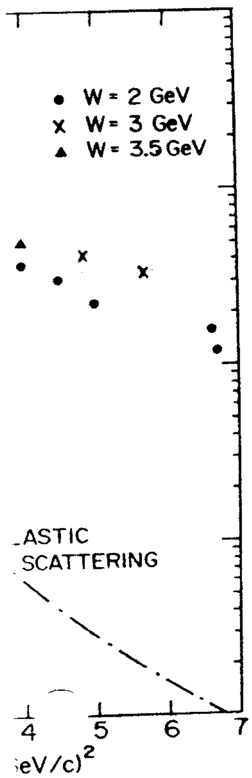

scattering (Ref. 3). The double dif-
the Mott cross section for elastic
')/σ_{Mott}, is plotted as a function
ocess is depicted in Fig. 1.2 . Note
ıre the energies of the incident and
gle. The data are shown for various
target system, W, and compared
ıuch more rapidly. See text for more

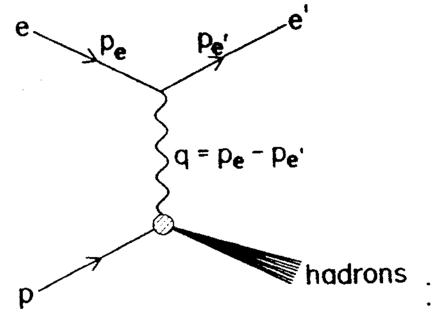

Figure 1.2 Feynman diagram for deep inelastic electron-proton scattering. The four-momenta are labelled on the diagram, with $q = (p_e - p_e')$.

by the atomic nucleus. To elaborate a little more on this point, consider the elementary process

$$e + P \to e' + X \quad , \tag{1.1.1}$$

as depicted in Fig. 1.2 . Such Feynman diagrams will be used throughout the book. In quantum field theory, there are well-defined rules of writing down the matrix-element of a Feynman diagram. We have labelled the four-momenta of the incoming and outgoing electrons by p_e and p_e', and the four momentum of the target proton by p. All leptons, so far as we know, are point-like Dirac particles. A proton, on the other hand, interacts strongly and has an internal structure of its own (like other baryons and mesons). This is shown by a dark blob at the proton vertex in the figure. Throughout this book, we use tha Bjorken-Drell convention of the metric, and natural units $\hbar = c = 1$. (The reader unfamiliar with this should first read the Appendix). In a deep inelastic process like (1.1.1), where a large amount of energy and momentum has been transferred to the target, the proton breaks up into hadrons X. The four-momentum transfer from the electron to the target is

$$q = p_e - p_e' \ .$$

Now, the central point is the following. In an inelastic process like this, there should be two independent variables, the energy loss $(E_e - E_e')$ and the three momentum transfer $\mathbf{q}$ on which the inclusive scattering cross-section should depend. Instead, it is found that the cross-section depends, to a good degree, only on *one* variable $x = (Q^2/2M\nu)$, where $Q^2 = -q^2$, and $\nu = E_e - E_e'$ in the labratory frame. This is the signature of an *elastic* scattering of the electron from a free, point-like constituent that is carrying a fraction x of the four momentum of the proton. This is called

"Bjorken[4] scaling" because the measured cross-section, at Q^2 and ν, is the same as the cross-section at Q'^2 and ν', provided the variables are scaled as

$$\frac{\nu}{\nu'} = \frac{Q^2}{Q'^2} \,. \tag{1.1.2}$$

It is this observation of scaling in the original experiment that implied the existence of the point-like constituents of the nucleon, called partons[4]. The experiment also pointed to what is called "asymptotic freedom" — that for large Q^2, the partons seem to be moving freely of each other — interacting only weakly. The rush was on for the search of a theory of strong interaction that waned in strength at shorter distances — and QCD, (Quantum chromodynamics) came along.

Exercise 1.1

(a) Consider Fig. 1.2 . From the definition of the four momentum p, we have

$$p_\mu p^\mu = p \cdot p = p_0^2 - \mathbf{p} \cdot \mathbf{p} = M^2 \,.$$

Show that the four momentum transfer $q = (p_e - p_e')$ obeys the equation (θ is the scattering angle)

$$q^2 = -4E_e E_e' \sin^2 \theta/2 \quad ,$$

provided that E_e, $E_e' \gg m_e$, the rest mass of the electron. For a real photon, $q^2 = 0$. A virtual photon is characterized by $q^2 \neq 0$. For $q^2 < 0$, as in this case, it is called space-like, and for $q^2 > 0$ it is time-like.

(b) Consider the elastic scattering process $e + P \to e' + P'$, as shown in Fig. 1.3 . Show that now $q^2 = -2p \cdot q$. In the labratory frame, the proton is at rest, and in this situation prove that

$$x = \frac{Q^2}{2M\nu} = 1 \quad ,$$

where

$$Q^2 = -q^2 \quad , \quad \text{and} \quad \nu = E_e - E_e' \,.$$

To appreciate the significance of the scaling variable $x = (Q^2/2M\nu)$, assume that the proton is made up of point-like constituents, each having a mass m, and carrying a fraction ξp of its momentum (see Fig. 1.4). A

Figure 1.3 Elastic e-P sc

constituent absorbs the vi
elastically. In practice, si
with other constituents, i
tent, and the encounter is
momentum of the struck

This is a Lorentz-invariant
In the labratory frame, $p \cdot$

ξp

Figure 1.4 The scattering
absorption.

red cross-section, at Q^2 and ν, is
ınd ν', provided the variables are

2
$\overline{}2$ · (1.1.2)

original experiment that implied
nts of the nucleon, called partons[4].
ıs called "asymptotic freedom" —
o be moving freely of each other
was on for the search of a theory
ength at shorter distances — and
ne along.

ıtion of the four momentum p, we

$- \mathbf{p} \cdot \mathbf{p} = M^2$.

ısfer $q = (p_e - p'_e)$ obeys the equa-

$\sin^2 \theta/2$,

st mass of the electron. For a real
ı is characterized by $q^2 \neq 0$. For
d ace-like, and for $q^2 > 0$ it is

cess $e + P \to e' + P'$, as shown in
$p \cdot q$. In the labratory frame, the
ion prove that

$= 1$,

d $\nu = E_e - E'_e$.

ıe scaling variable $x = (Q^2/2M\nu)$,
ıoint-like constituents, each having
of its momentum (see Fig. 1.4). A

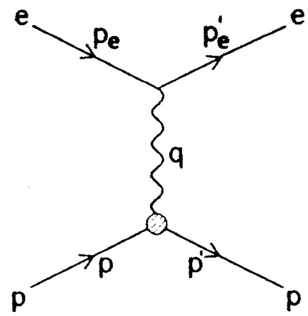

Figure 1.3 Elastic e-P scattering.

constituent absorbs the virtual photon of momentum q and gets scattered elastically. In practice, since it is part of a bound system, and interacts with other constituents, its momentum would be smeared to some extent, and the encounter is "quasielastic". Ignoring such effects, the four momentum of the struck parton is $(\xi p + q)$, and in Lab

$\xi^2 M^2 - Q^2 + 2\xi M\nu + 0 =$

$$(\xi p + q)^2 = m^2 ,$$

$$\therefore \quad \xi = \frac{Q^2}{2(p \cdot q)} .$$

This is a Lorentz-invariant quantity, and may be evaluated in any frame. In the labratory frame, $p \cdot q = M\nu$, and we see that

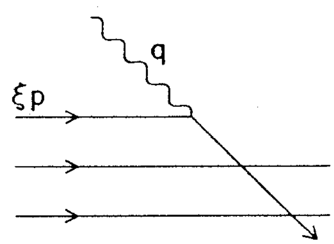

Figure 1.4 The scattering of a parton in the nucleon via a virtual photon absorption.

$$\frac{Q^2}{2(p \cdot q)} = \frac{Q^2}{2M\nu} = x \ . \qquad (1.1.3)$$

When the conditions Q^2 and $M\nu \gg M^2$ are met, the process is called deep inelastic, and we may identify x with the fractional four momentum ξ. This will have important implications in the interpretations of the data. In Fig. 1.4, the struck constituent cannot get loose by itself, unlike in nuclear physics where a nucleon, as a constituent of a nucleus, may be knocked out. The free partons are never seen in isolation, so the underlying theory, in addition to being asymptotically free, must be confining the constituents. The constituents and the quanta that they radiate and exchange carry color charge in the theory, and it is arranged that only color-neutral objects may be free. The struck constituent in Fig. 1.4, in stretching out to longer distances, will drag the others with it due to this confining mechanism. It will also create other $(q\bar{q})$-pairs from the vacuum to use up the energy deposited by the scattered electron. The (color-neutral) hadrons that are formed will come out in a jet following the trail of the struck parton, as shown shematically in Fig. 1.2 .

Before getting a little more quantitative, it is worth recounting another set of experiments[5,6] with incident neutrinos and antineutrinos that were even more spectacular in import. In the deep inelastic processes

$$\begin{aligned} \nu_\mu + N &\rightarrow \mu^- + X \\ \bar{\nu}_\mu + N &\rightarrow \mu^+ + X \end{aligned} \qquad (1.1.4)$$

the total inclusive cross-section was measured (identifying the outgoing muon in a giant bubble chamber). A burst of $\sim 10^9$ ν_μ or $\bar{\nu}_\mu$ (from decay of $\pi^+ \rightarrow \mu^+ + \nu_\mu$, or $\pi^- \rightarrow \mu^- + \bar{\nu}_\mu$) at intervals of a few seconds traversed several detectors placed in series. Typically, the energy of the ν's is $\sim 200\,\mathrm{GeV}$, although in the original experiments at CERN and Fermilab the energies were much less. In every burst, a handful of the neutrinos undergo the interaction (1.1.4) in the bubble chamber. A very readable account of these experiments is given in a popular article by Perkins[7]. The spectacular linear rise in the total cross-section $\sigma(\nu N)$ or $\sigma(\bar{\nu}N)$ with the incident energy is shown in Fig. 1.5 . This is again a signature that the ν $(\bar{\nu})$ is getting elastically scattered by point-like objects in the nucleon. Such rising cross-sections are observed, for example, in the elastic collisions of ν_e on electrons. A lepton-lepton scattering is mediated by the exchange of heavy bosons ($W^\pm$ and Z_0), and may be considered to be due to zero-range weak interactions. The Coulomb interaction between two charges e in momentum space is $e^2/4\pi q^2$. For weak-interaction, we

may replace e by a weak
nator changes to $(q^2$
Section 5.3). For $M_W^2 \gg$
(F is after Fermi) with
interaction[8]. The experim

$G_F M$

We show the zero-range i
There is no unknown "blo
ticles. The total cross se
as

where $s = (p_\nu + p_e)^2$. This
and the cross section is o
plying by the available ph

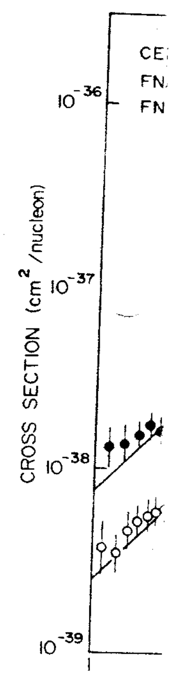

Figure 1.5 Total cross secti
nucleons (after Perkins, ref. 7).

$$= \ldots \qquad (1.1.3)$$

are met, the process is called
ith the fractional four momen-
ons in the interpretations of the
annot get loose by itself, unlike
onstituent of a nucleus, may be
seen in isolation, so the under-
totically free, must be confining
e quanta that they radiate and
ry, and it is arranged that only
truck constituent in Fig. 1.4, in
drag the others with it due to
reate other ($q\bar{q}$)-pairs from the
by the scattered electron. The
will come out in a jet following
hematically in Fig. 1.2 .
ative, it is worth recounting an-
neutrinos and antineutrinos that
n the deep inelastic processes

$$+ X \qquad (1.1.4)$$
$$+ X$$

asured (identifying the outgoing
rs $\sim 10^9$ ν_μ or $\bar{\nu}_\mu$ (from decay
at intervals of a few seconds tra-
Typically, the energy of the ν's is
eriments at CERN and Fermilab
urst, a handful of the neutrinos
ubble chamber. A very readable
a popular article by Perkins[7]. The
section $\sigma(\nu N)$ or $\sigma(\bar{\nu} N)$ with the
This is again a signature that the
point-like objects in the nucleon.
for example, in the elastic colli-
on scattering is mediated by the
0), and may be considered to be
he Coulomb interaction between
$^2/4\pi q^2$. For weak-interaction, we

may replace e by a weak dimensionless charge g, and q^2 in the denominator changes to $(q^2 - M_W^2)$. (A more sophisticated account is given in Section 5.3). For $M_W^2 \gg Q^2$, the net result is a coupling constant G_F (F is after Fermi) with dimensions of M^{-2} (*i.e.*, L^2) in a zero-range interaction[8]. The experimental value of G_F is found to be

$$G_F M_p^2 = (1.026 \pm 0.001) \times 10^{-5} \ . \qquad (1.1.5)$$

We show the zero-range interaction in the Feynman diagram of Fig. 1.6 . There is no unknown "blob" at the vertex because leptons are point particles. The total cross section, on dimensional ground alone, should go as

$$\sigma(\nu_e e^-) \sim G_F^2 s \quad , \qquad (1.1.6)$$

where $s = (p_\nu + p_e)^2$. This is so since the amplitude of the diagram $\propto G_F$, and the cross section is obtained by squaring the amplitude and multiplying by the available phase space. The quantity s is the only Lorentz-

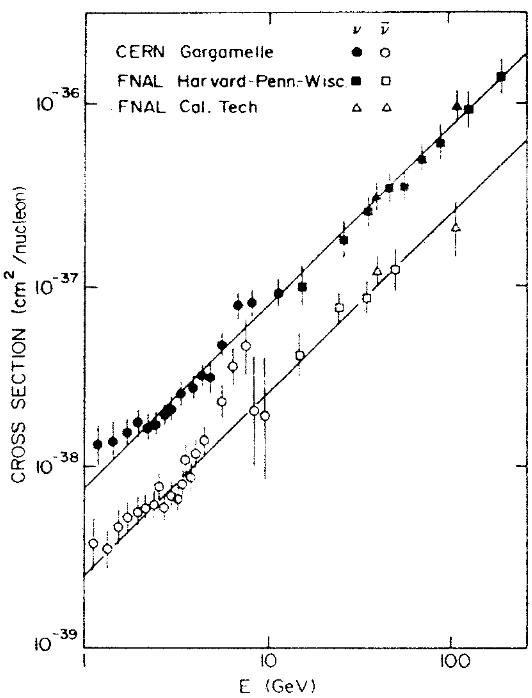

Figure 1.5 Total cross sections for neutrino and antineutrino scattering on nucleons (after Perkins, ref. 7).

invariant nonnegative variable in the incoming channel, and enters in the phase space calculation. Note in (1.1.6) that σ has the correct dimension of L^2. In the Labratory frame (electron at rest)

$$s = p_\nu^2 + p_e^2 + 2p_\nu \cdot p_e \approx 2E_\nu m_e \quad ,$$

so the linear dependence in σ is obtained. This is why the linear rise in $\sigma(\nu N)$ or $\sigma(\bar{\nu} N)$, shown in Fig. 1.5, is so informative. The neutrino does not regard the nucleon itself as a point. Indeed, from reactions like

$$\nu_\mu d \to \mu^- pp \quad ,$$

the axial size of the nucleon may be deduced (see Fig. 2.12). It must, therefore, have point-like constituents. More may be learnt by noting, in Fig. 1.5, that $\sigma(\nu_\mu N)$ is more than twice as big as $\sigma(\bar{\nu}_\mu N)$ at a given energy. Indeed, in the electron-neutrino problem, the same trend is observed, and the cross-section $\sigma(\nu_e e^- \to \nu_e e^-)$ is three times $\sigma(\bar{\nu}_e e^- \to \bar{\nu}_e e^-)$. This is because the struck electron is a Dirac spin-$\frac{1}{2}$ particle, as are the ν, $\bar{\nu}$. The helicity of the particles in the interaction is conserved and a $(V - A)$ theory yields the factor of 3 easily (see Section 2.6, 2.7 and ref. 9). In the inelastic (νN) scattering, $\sigma(\nu_\mu N)$ is not quite three times $\sigma(\bar{\nu}_\mu N)$, but the difference is due to some other degrees of freedom like the $q\bar{q}$ pairs in the nucleon. These may arise from the "gluons" that are emitted in the bremsstrahlung of the spin-$\frac{1}{2}$ contituents. If the point-like constituents off which the ν $(\bar{\nu})$ scatter had any other intrinsic spin, $\sigma(\nu_\mu N) \approx \sigma(\bar{\nu}_\mu N)$. Thus the experiments involving neutrino's tell us of point-like spin-$\frac{1}{2}$ constituents inside the nucleon. To delve a little more, we must now learn

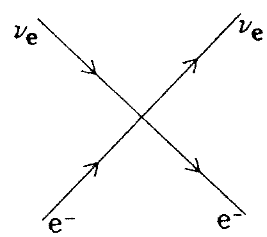

Figure 1.6 Electron-neutrino scattering due to an effective zero-range interaction

about elastic form factors and inelastic structure functions of the nucleon, which we proceed to do in the next section. One may then deduce from the experimental data that the spin-$\frac{1}{2}$ constituents (including the $q\bar{q}$ sea) only carry about 54 % of the proton's momentum. It is inferred that the quanta of the color field, gluons, must be carrying the rest of the momentum. The gluons do not interact directly with any colorless object like electrons or neutrinos.

1.2 FORM FACTORS AND STRUCTURE FUNCTIONS

In this section we briefly review some aspects of the above topics that are relevent to the study of nucleon structure. The subject of deep inelstic scattering and structure functions has been covered very well in texts by Halzen and Martin[9], and in Close[10]. We start with elastic electron-proton scattering. In nuclear physics, this has been very fruitful in giving the profiles of the charge distribution of nuclei[11]. Consider the elastic scattering of an electron from a static, spinless charge distribution which is taken to be infinitely heavy. The target does not recoil and is not internally excited and so cannot absorb any energy. In this situation (see Fig. 1.3)

$$q^2 = (p_e - p_e')^2 = -\mathbf{q}^2$$

$$\therefore \quad Q^2 = \mathbf{q}^2 \, .$$

The elastic differential cross-section of the electron is given by

$$\left(\frac{d\sigma}{d\Omega}\right)_{eP\to eP} = \left(\frac{d\sigma}{d\Omega}\right)_{Mott} |F(\mathbf{q})|^2 \, . \tag{1.2.1}$$

The cross section $\left(\frac{d\sigma}{d\Omega}\right)_{Mott}$ is what one would get from a spin-less point charge, and its expression will be given shortly. The information of the charge distribution is contained in the form factor $F(\mathbf{q})$, given by

$$F(\mathbf{q}) = \int \rho(\mathbf{r}) e^{i\mathbf{q}\cdot\mathbf{r}} \, d^3r \quad , \tag{1.2.2}$$

where $\rho(\mathbf{r})$ is the charge density with the normalization $\int \rho(\mathbf{r})\, d^3r = 1$. The most interesting point here is that the differential cross-section has a diffraction pattern as a function of $|\mathbf{q}|$ or θ if $\rho(\mathbf{r})$ has an edge, or a shoulder at the surface. The other interesting point is that $|F(\mathbf{q})|^2$ falls off very rapidly with Q^2, and more so for a bigger size. For a point distribution, of course, $F(\mathbf{q}) = 1$.

Exercise 1.2 assume $M \gg E \Rightarrow Q^2 = q_3^2$

(a) Consider a spherically symmetric uniform charge distribution with a sharp edge at the surface at $r = R$, *i.e.*,

$$\rho(r) = \rho_0 \quad , \quad r \leq R \quad ; \quad \rho(r) = 0 \quad \text{for} \quad r > R \; .$$

Show that

$$F(Q^2) = \frac{4\pi\rho_0}{Q^3}\left[\sin(QR) - (QR)\cos(QR)\right] \; .$$

(b) Next take a smooth charge distribution

$$\rho(r) = \frac{m^3}{8\pi} e^{-mr} \; .$$

Show that

$$F(Q^2) = \left(1 + \frac{Q^2}{m^2}\right)^{-2} \; .$$

This is called the dipole form. Note that for large R (or small m) $F(Q^2)$ falls off faster.

These point are well illustrated in nuclear form-factors. The charge form-factor of the ^{3}He nucleus is shown[12] in Fig. 1.7, and has an oscillatory pattern. In contrast, the deutron charge form-factor has no such undulations and falls off smoothly[13]. (Actually the "charge" form factor plotted here also contains a small magnetic contribution). We shall see that for the proton $F(q^2)$ looks more like the deutron than ^{3}He, indicating that its charge distribution has no shoulder or edge. For the elastic eP-scatering of Fig. 1.3, the differential cross-section is given by the Rosenbluth formula,

$$\left(\frac{d\sigma}{d\Omega}\right)_{eP\to eP} = \left(\frac{d\sigma}{d\Omega}\right)_{Mott} \cdot \frac{E_e'}{E_e}\left[\frac{G_E^{P} + \tau G_M^{P}}{(1+\tau)} + 2\tau (G_M^P)^2 \tan^2\frac{\theta}{2}\right] \; , \tag{1.2.3}$$

where $\tau = Q^2/4M_P^2$, θ is the scattering angle in the labratory frame,

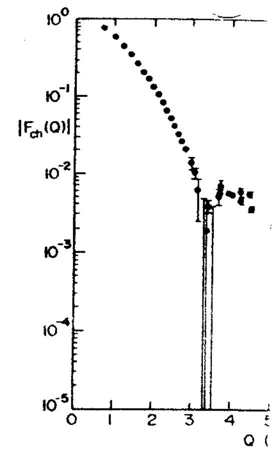

Figure 1.7 The char
of four-momentum Q^2
about 1 GeV^2. For re
Phys., **A446**, 151c (1

and $G_E^P(q^2)$ and G_M^P(
proton. The same fo
form factors G_E^n, G_M^n.
m_e, corresponds, as b
less point charg

Note that the elastic
able q^2. The Rosenbl
exchange assumption,
moments of the proto
from experiments wit
normalized to these v

We have rounded off
point. The nuclear m

$Q^2 = q_3^2$

orm charge distribution with a

?.,

$r) = 0 \quad \text{for} \quad r > R$.

$- (QR)\cos(QR)]$.

n

$-mr$.

$\left.\frac{Q^2}{m^2}\right)^{-2}$.

that for large R (or small m)

clear form-factors. The charge
ı Fig. 1.7, and has an oscillatory
or ıctor has no such undula-
1e "charge" form factor plotted
ibution). We shall see that for
on than ^{3}He, indicating that its
. For the elastic eP-scatering of
/en by the Rosenbluth formula,

$\frac{\tau G_M^P}{\cdot \tau)} + 2\tau(G_M^P)^2 \tan^2 \frac{\theta}{2}\Big]$, (1.2.3)

angle in the labratory frame,

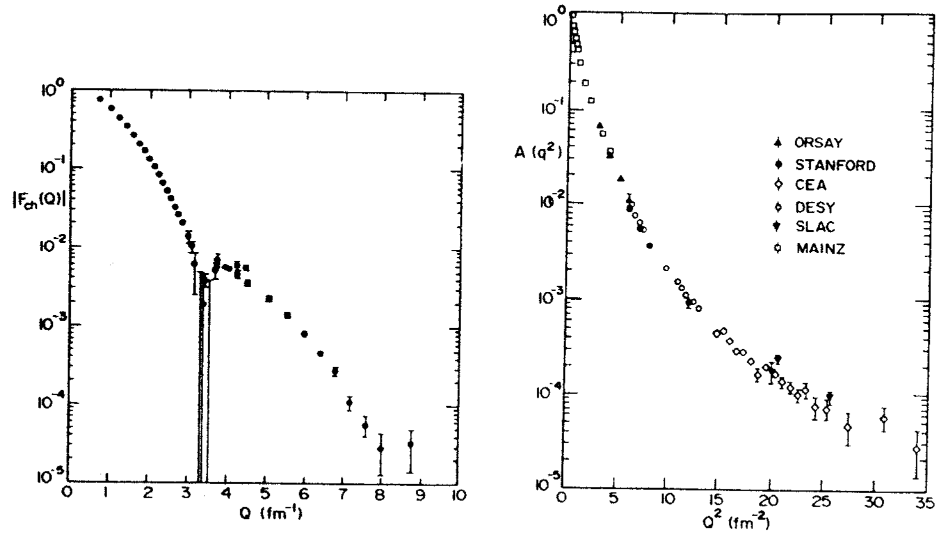

Figure 1.7 The charge form factors of (a) ^{3}He and (b) deuteron as a function of four-momentum Q^2 in fm^{-2}. Note that $Q^2 = 25\,\text{fm}^{-2}$ corresponds to only about $1\,\text{GeV}^2$. For references to experimental data, see S. Platchkov, *Nucl. Phys.*, **A446**, 151c (1985).

and $G_E^P(q^2)$ and $G_M^P(q^2)$ are the electric and magnetic form-factors of the proton. The same formula holds good for the neutron, with appropriate form factors G_E^n, G_M^n. The Mott cross-section, $(\frac{d\sigma}{d\Omega})_{Mott}$, for incident $E_e \gg m_e$, corresponds, as before, to the scattering from an infinitely heavy spin-less point charge (here $Z = 1$):

$$\left(\frac{d\sigma}{d\Omega}\right)_{Mott} = \frac{\alpha^2}{4E_e^2 \sin^4 \theta/2} . \tag{1.2.4}$$

Note that the elastic form-factors in Eq. (1.2.3) depend only on one variable q^2. The Rosenbluth formula (1.2.3), derived under the one-photon-exchange assumption, fits the experimental points very well. The magnetic moments of the proton and the neutron are known extremely accurately from experiments with real photons ($q^2 = 0$), and $G_M^P(0)$ and $G_M^N(0)$ are normalized to these values:

$$\begin{aligned} G_M^P(0) &= \mu_P = 2.7928\,\mu_0 \\ G_M^N(0) &= \mu_N = -1.9131\,\mu_0 . \end{aligned} \tag{1.2.5}$$

We have rounded off these values of μ_P and μ_N at the fourth decimal point. The nuclear magneton is always defined as $\mu_0 = e/2M_P$, where

e and M_P are the charge and the mass of the proton. From Eq. (1.2.3), we see that a plot of the ratio $\left(\frac{d\sigma}{d\Omega}\right)_{eN\to eN} / \left(\frac{d\sigma}{d\Omega}\right)_{Mott}$ against $\tan^2 \theta/2$ for fixed $\tau = Q^2/4M_P^2$ yields both G_E^2 and G_M^2. The experimental points for $G_E^P(q^2)$ are shown in Fig. 1.8 . A comparison with the deuteron (Fig. 1.7) shows that it falls off much more slowly with Q^2. The proton form factor may be fitted well by the dipole form (see Ex. 1.2 (b))

$$G_E^P(q^2) = \left(1 - \frac{q^2}{0.71}\right)^{-2} . \tag{1.2.6}$$

The mean-square charge radius is defined by

$$\langle r^2 \rangle_{\text{charge}} = -6\left(\frac{dG_E}{dQ^2}\right)\bigg|_{Q^2=0} . \tag{1.2.7}$$

One should not use the dipole-form (1.2.6), which is only an overall fit with one parameter, to determine the root-mean square charge radius.

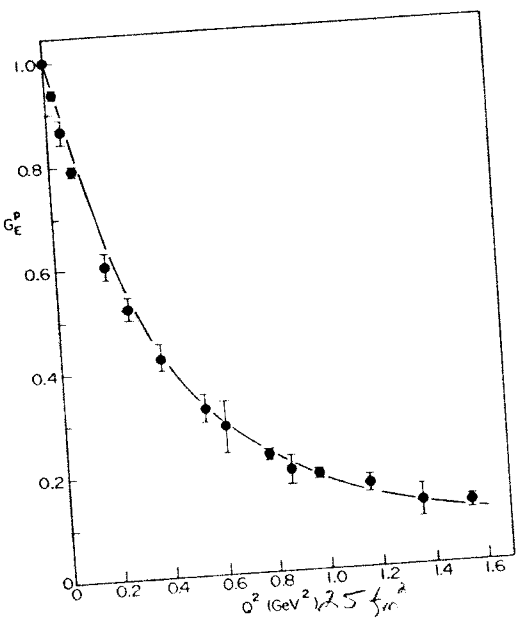

Figure 1.8 The elastic form factor, G_E^P, of a proton plotted as a function of Q^2. The dipole fit (Eq. 1.2.6) is shown for comparison. The experimental data is from S. Blatnik and N. Zovko *Acta Phys. Austriaca*, **39**, 62 (1974).

The latter is very sensiti
yields the result[14]

Although the electric an
inaccurately extracted f
dius is well determined
electrons:

The negative sign is int
derance of negative elec
not discuss the poor dat
that[11]

The electric form factor
Q^2 in Fig. 1.9 .

The electric form f
relation to the vector-do
in Fig. 7.4 . For complet
radius[17],

It should be realized
on the probe. For an elec
that is obtained. Bu
netically, but rather t
like $\nu_\mu d \to pp\mu^-$, the axi
axial $r.m.s.$ radius of th

which is substantially sm
mean square radius of th
Eqs. (1.2.8) and (1.2.9),

Now we come to ine
considered in Section 1.1

of the proton. From Eq. (1.2.3), $\mu\left(\frac{d\sigma}{d\Omega}\right)_{Mott}$ against $\tan^2 \theta/2$ for ... he experimental points for ... rison with the deutron (Fig. 1.7) with Q^2. The proton form factor ee Ex. 1.2 (b))

$$\left.\frac{q^2}{0.71}\right)^{-2} . \qquad (1.2.6)$$

ed by

$$\left.\frac{G_E}{dQ^2}\right)\Big|_{Q^2=0} . \qquad (1.2.7)$$

.2.6), which is only an overall fit root-mean square charge radius.

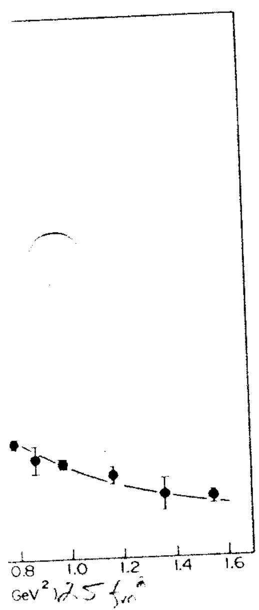

G_E^P, of a proton plotted as a function of for comparison. The experimental data *Phys. Austriaca*, **39**, 62 (1974).

The latter is very sensitive to the slope at $Q^2 = 0$. A very careful analysis yields the result[14]

$$\langle r_p^2 \rangle^{1/2} = 0.862\,(12)\,\text{fm} . \qquad (1.2.8)$$

Although the electric and magnetic form factors of the neutron are rather inaccurately extracted from electron-deutron data, its electric charge radius is well determined[15] from the scattering of slow neutrons off atomic electrons:

$$\langle r_n^2 \rangle_{\text{charge}} = -0.1192\,(18)\,\text{fm}^2 . \qquad (1.2.9)$$

The negative sign is interesting, and may be interpreted as the preponderance of negative electric charge in the tail of the ditribution. We do not discuss the poor data in the neutron form factor, except to point out that[11]

$$\frac{1}{\mu_n} G_M^n(q^2) \approx \frac{1}{\mu_p} G_M^P(q^2) \approx G_E^P(q^2) . \qquad (1.2.10)$$

The electric form factor of the neutron[16], G_E^n, is shown as a function of Q^2 in Fig. 1.9 .

The electric form factor of the pion is discussed in Section 7.1 in relation to the vector-dominance model. The experimental data are shown in Fig. 7.4 . For completeness here we only quote the experimental *r.m.s.* radius[17],

$$\langle r_\pi^2 \rangle_{\text{charge}}^{1/2} = (0.66 \pm 0.01)\,\text{fm} . \qquad (1.2.11)$$

It should be realized that the size and the density of a hadron depends on the probe. For an electromagnetic probe, it is the electric charge radius that is obtained. But a probe like a neutrino does not interact electromagnetically, but rather by the weak current (see Section 2.7). From a reaction like $\nu_\mu d \to pp\mu^-$, the axial form factor is determined (see Fig. 2.12). The axial *r.m.s.* radius of the nucleon is found to be[18]

$$\langle r_N^2 \rangle_{\text{axial}}^{1/2} = (0.68 \pm 0.02)\,\text{fm} \quad , \qquad (1.2.12)$$

which is substantially smaller than the electric charge radius. The isoscalar mean square radius of the nucleon is a sum of $\left(\langle r_P^2 \rangle_{\text{ch}} + \langle r_n^2 \rangle_{\text{ch}}\right)$, and from Eqs. (1.2.8) and (1.2.9), is given by

$$\langle r_N^2 \rangle_{\text{isoscalar}}^{1/2} = 0.79\,\text{fm} . \qquad (1.2.13)$$

Now we come to inelastic electron scattering off a nucleon that was considered in Section 1.1 . With increasing beam energy, the nucleon may

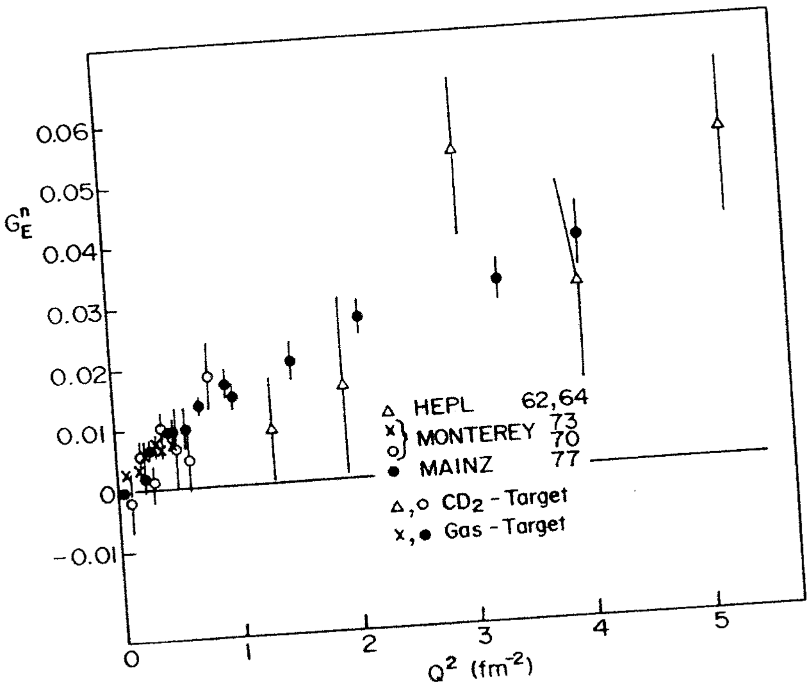

Figure 1.9 The electric form factor G_E^n of the neutron (After Simon *et al.*, ref. 16).

get internally excited to its resonant states which then decay strongly to hadrons. With still greater beam energy, the nucelon breaks up into a jet of hadrons, as described earlier (see Fig. 1.2):

$$e + P \to e' + X \quad ,$$

where X stands for the hadrons. To find the inclusive double differential cross-section, one counts the scattered electrons e' between the scattering angles θ and $\theta + \delta\theta$ in the energy range E_e' and $E_e' + \delta E_e'$, without worrying about the hadrons X. The formal expression for the double-differential cross-section[10] of deep inelastic scattering looks very similar to the elastic Rosenbluth formula (1.2.3),

$$\left[\frac{d^2\sigma}{dE_e' d\Omega}\right]_{eP\to ex} = \left(\frac{d\sigma}{d\Omega}\right)_{Mott} [W_2^P(\nu, Q^2) + 2W_1^P(\nu, Q^2)\tan^2 \theta/2] \ . \tag{1.2.14}$$

We see that the from fact
by two "structure fun
energy-loss ν in the la
arguements of current con
are only two such structur
scattering, weak currents
there is one more structu
in the previous section in F
falls of much more slowly
the Mott cross-section. T
deep inelastic region. Sup
valence quarks in the pro
where M is the proton ma
"elastic" scattering of suc
this idealized model, only

Q

Of course, one may expect
of the "Fermi motion" of
other partons, the $q\bar{q}$ sea.
of x where gluon bremsstr
presence of the $q\bar{q}$ pairs has
by taking the differen
eliminated. The expe
functions, $(F_2^P - F_2^n)$, whe
trate and confirm Eq. (1.2.
Soon we shall see tha
(1.2.14) is proportional to
and the quasi-elastic peak

e

are also shown in Fig. 1.1
scatters elastically with th
knocks it out. From our pr
contituents, each with mas
appear at $x = Q^2/2M_d \approx$
smeared by the Fermi moti

We see that the from factors of elastic scattering have now been replaced by two "structure functions" W_1 and W_2, which in general depend on the energy-loss ν in the labratory frame, and Q^2. One can show, from general arguements of current conservation and invariance properties, that there are only two such structure functions in e-N and μ-N scattering. For ν-N scattering, weak currents containing axial-vector parts are involved, and there is one more structure function W_3. Experimentally, as emphasized in the previous section in Fig. 1.1, one finds that the inelastic cross-section falls of much more slowly than the elastic one — indeed it is more like the Mott cross-section. This leads to Bjorken scaling, Eq. (1.1.2), in the deep inelastic region. Suppose, for simplicity, that there are only three valence quarks in the proton, each with a "constituent" mass $m_q = M/3$, where M is the proton mass (we drop the subscript P from now on). The "elastic" scattering of such a "parton" with the electron takes place, in this idealized model, only for $Q^2 = Q_1^2$, such that

$$Q_1^2 = 2m_q\nu = 2(M/3)\nu \ .$$

$$\therefore \qquad x = x_1 = \frac{Q_1^2}{2M\nu} = \frac{1}{3} \ . \tag{1.2.15}$$

Of course, one may expect this peak to smear out because of the neglect of the "Fermi motion" of these quarks, and more importantly, from the other partons, the $q\bar{q}$ sea. The latter are more copious at smaller values of x where gluon bremsstrahlung is more effective. If we assume that the presence of the $q\bar{q}$ pairs has the same effect in e-P and e-n scattering, then by taking the difference in these two cross-sections, the sea-effect may be eliminated. The experimental data for the difference[19] in the structure functions, $(F_2^P - F_2^n)$, where $F_2 = W_2/\nu$, are shown in Fig. 1.10 to illustrate and confirm Eq. (1.2.15).

Soon we shall see that to a good approximation, the cross-section (1.2.14) is proportional to F_2. Following Atwood[19], the elastic e-P peak and the quasi-elastic peak in the reaction

$$e + d \rightarrow e + P + n \quad , \tag{1.2.16}$$

are also shown in Fig. 1.10 . In reaction (1.2.16), the incoming electron scatters elastically with the proton in the loosely bound deutron, and knocks it out. From our previous arguement, since the deuteron has two contituents, each with mass M, and $M_d \approx 2M$, we expect the peak to appear at $x = Q^2/2M_d \approx \frac{1}{2}$. Of course, such a "quasi-elastic" peak is smeared by the Fermi motion of the nucleons. For comparison, the elastic

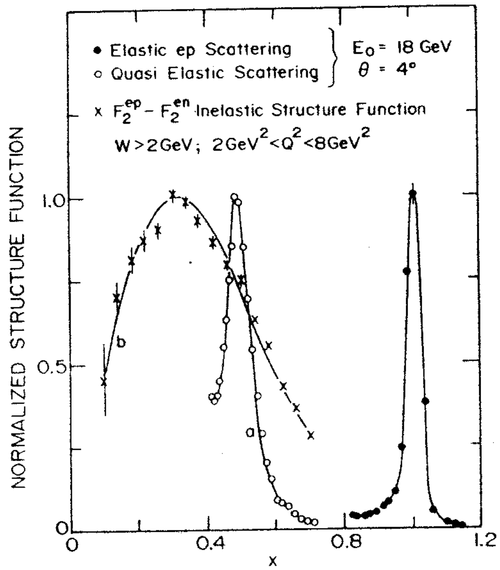

Figure 1.10 Quasi-elastic electron scattering from (a) nucleons in a deuteron, (b) partons in nucleon. The normalized structure functions are plotted against x, as defined in the text. For comparison, the elastic e-P data are also shown in (c). The e-P and e-D data are for incident electron energy $E_e = 18\,\mathrm{GeV}$, and scattering angle $\theta = 4°$. In (b), $(F_2^{eP} - F_2^{en})$ is plotted to eliminate the sea-quark contribution. The data are for $2\,\mathrm{GeV}^2 < Q^2 < 8\,\mathrm{GeV}^2$, with invariant mass $W > 2\,\mathrm{GeV}$ (after Atwood, ref. 19).

peak for $e + P \to e + P$ is also shown in Fig. 1.9 . Since the proton as a whole acts as one constituent in this reaction, the peak in this case comes at $x = Q^2/2M\nu = 1$. The reader should figure out the reason for the spread about $x = 1$ in this case. The broad peak in $(F_2^P - F_2^n)$ in Fig. 1.10 about $x = Q^2/2M\nu \approx \frac{1}{3}$ does suggest that there are three contituent quarks in the nucleon. It confirms the simple picture of the electron being elastically scattered off the valence quark, and the subsequent hadronization (Section 1.1). The electron scattering data are supplemented by the more energetic muon (and also neutrino) results. For example, $(F_2^P - F_2^n)$ from muon-scattering[20] is shown in Fig. 1.11 .

We now describe the parton model in a form introduced by Feynman[4]. In this model, the high-energy incident lepton sees the nucleon as an assembly of long-lived, point-like partons. The deep inelastic lepton-nucleon

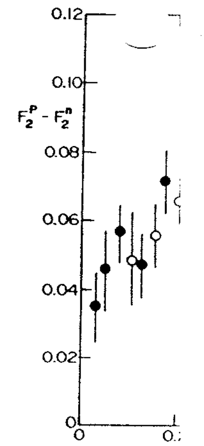

Figure 1.11 The variation of
x. The dark dots are the EMC
circles are SLAC-MIT data (2

cross-section is found by an
cross sections. The interesti
a double role. It may be int
momentum carried by the st
the structure-functions W_2 a
rally because only elast
are involved in the dee
large longitudinal momentu
momentum

where E and $\mathbf{p}$ are the energy
mass of the constituent, m_q,

$m_q = \sqrt{}$

where M is the nucleon mass
value between 0 and 1. Let t
fraction of momentum betwe

$\sum_i$

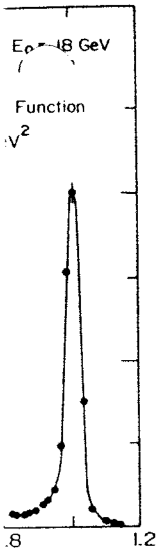

from (a) nucleons in a deuteron,
ire functions are plotted against
lastic e-P data are also shown in
ctron energy $E_\epsilon = 18\,\text{GeV}$, and
i is plotted to eliminate the sea-
$< Q^2 < 8\,\text{GeV}^2$, with invariant

F 1.9 . Since the proton as
acuon, the peak in this case
should figure out the reason
The broad peak in $(F_2^P - F_2^n)$
s suggest that there are three
rms the simple picture of the
valence quark, and the subse-
ctron scattering data are sup-
and also neutrino) results. For
[20] is shown in Fig. 1.11 .
form introduced by Feynman[4].
ton sees the nucleon as an as-
ie deep inelastic lepton-nucleon

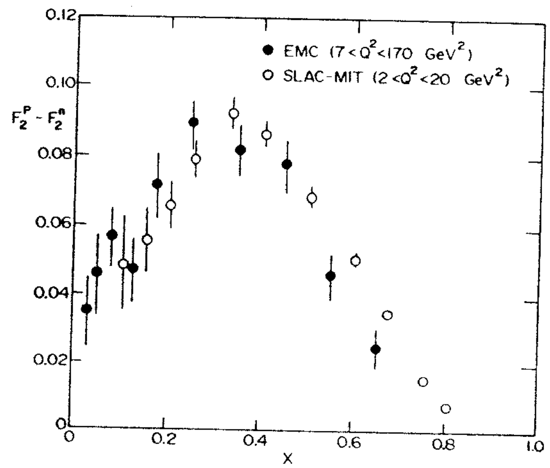

Figure 1.11 The variation of $(F_2^P - F_2^n)$, averaged over Q^2, as a function of x. The dark dots are the EMC muon data $(7 < Q^2 < 170\,\text{GeV}^2)$, and the open circles are SLAC-MIT data $(2 < Q^2 < 20\,\text{GeV}^2)$ (after Aubert *et al.*, ref. 20).

cross-section is found by an *incoherent* sum of the elastic lepton-parton cross sections. The interesting point is that the Bjorken variable x plays a double role. It may be interpreted, from Eq. (1.1.3), as the fractional momentum carried by the struck parton. It is also the variable on which the structure-functions W_2 and W_1 mainly depend. Scaling follows naturally because only elastic scatterings between the partons and electrons are involved in the deep inelastic process. In a frame of reference with large longitudinal momentum (Fig. 1.4), the struck parton has a four-momentum

$$\xi p = (\xi E, \xi \mathbf{p}) \quad ,$$

where E and $\mathbf{p}$ are the energy and momentum of the nucleon. The effective mass of the constituent, m_q, is

$$m_q = \sqrt{(\xi E)^2 - (\xi \mathbf{p})^2} = \xi M \quad , \tag{1.2.17}$$

where M is the nucleon mass. The fraction ξ, of course, may take on any value between 0 and 1. Let the probability that the ith parton carries a fraction of momentum between ξ and $\xi + d\xi$ be $f_i(\xi)\,d\xi$, then

$$\sum_i \int_0^1 d\xi\, \xi f_i(\xi) = 1 \ . \tag{1.2.18}$$

This merely states that all the fractions add up to yield unity, and no momentum is lost. However, for the struck parton, ξ may be identified with the Bjorken variable $x = Q^2/2M\nu$ of scattering. A look at the Rosenbluth formula, Eq. (1.2.3), for a point charge ($G_E = G_M = 1$) will show that the structure functions of a parton (of mass m_q, charge e_q) are of the form

$$W_2^q = e_q^2\delta\left(\nu - \frac{Q^2}{2m_q}\right) \quad , \quad W_1^q = e_q^2\frac{Q^2}{4m_q^2}\delta\left(\nu - \frac{Q^2}{2m_q}\right) .$$

We have obtained the above forms by comparing the point-Rosenbluth formula with Eq. (1.2.14), with the constraint that $\nu = Q^2/2m_q$. From the above equations, it is seen that

$$\nu W_2^q = e_q^2\delta\left(1 - \frac{Q^2}{2\xi M\nu}\right) \quad , \quad MW_1^q = e_q^2\frac{1}{2\xi^2}\frac{Q^2}{2M\nu}\left(1 - \frac{Q^2}{2\xi M\nu}\right) . \tag{1.2.19}$$

In the above equation, we have used the identity $\delta(ax) = \frac{1}{a}\delta(x)$, and Eq. (1.2.17). The structure functions of the nucleon are found by an incoherent sum over the partons, appropriately weighted by the momentum distribution function f_i,

$$F_2^N = \nu W_2^N = \int \sum_i e_i^2 f_i(\xi)\delta\left(1 - \frac{Q^2}{2\xi M\nu}\right) d\xi .$$

Putting, as before, $x = Q^2/2M\nu$,

$$F_2^N = \sum_i e_i^2 \int f_i(\xi)\delta\left(1 - \frac{x}{\xi}\right) d\xi \quad ,$$

or

$$F_2^N(x) = \nu W_2^N(x) = \sum_i e_i^2 x f_i(x) . \tag{1.2.20}$$

Similar algebra gives for $F_1^N(x)$,

$$F_1^N(x) = MW_1^N(x) = \tfrac{1}{2}\sum_i e_i^2 f_i(x) . \tag{1.2.21}$$

It thus follows, from Eq. (1.2.20) and (1.2.21), that

$$F_2^N(x) = 2xF_1^N(x) . \tag{1.2.22}$$

This is known as the Callen-Gross relation[21]. Experimentally the Callen-Gross relation is verified. This is also a confirmation that the partons that absorb the virtual photon are spin-$\frac{1}{2}$ objects. Note that in the Rosenbluth

formula (1.2.3), the secon
ing. In the absence of
Obviously, in this si
more detailed analysis m
the cross-section of transv
This ratio may be extrac
cally charged partons ha
by remembering that heli
(Ex. 2.15). We shall not c

Digression : The Lore double-d

Consider Fig. 1.2 for

It is convenient to define

$$s = (p + p_e)^2 \quad , \quad t$$

where p, p_e and p'_e are the
tron and the scattered ele
s, t and u are independent

$$s + t + u$$

where W is the invar
differential cross-section fo
the labratory frame in Eq.

$$\left(\frac{d^2\sigma}{dt\,du}\right)_{eP\to eX} = \frac{4\pi}{t}$$

Using the Callen-Gross rel

$$\left(\frac{d^2\sigma}{dt\,du}\right)_{eP}$$

Here x is defined by Eq. (1
is directly proportional to
shown in Fig. 1.12 . The Q

up to yield unity, and no mo-
to may be identified with
n look at the Rosenbluth
$= G_M = 1)$ will show that
m_q, charge e_q) are of the form

$$^2\frac{Q^2}{4m_q^2}\delta\left(\nu - \frac{Q^2}{2m_q}\right) .$$

paring the point-Rosenbluth
int that $\nu = Q^2/2m_q$. From

$$^2\frac{1}{2\xi^2}\frac{Q^2}{2M\nu}\left(1 - \frac{Q^2}{2\xi M\nu}\right) . \qquad (1.2.19)$$

identity $\delta(ax) = \frac{1}{a}\delta(x)$, and
nucleon are found by an inco-
weighted by the momentum

$$1 - \frac{Q^2}{2\xi M\nu}\Big) d\xi .$$

$$d\xi ,$$

$$e_i^2 x f_i(x) . \qquad (1.2.20)$$

$$\sum_i e_i^2 f_i(x) . \qquad (1.2.21)$$

21), that

$$x) . \qquad (1.2.22)$$

1. Experimentally the Callen-
rmation that the partons that
s. Note that in the Rosenbluth

formula (1.2.3), the second term with $\tan^2 \theta/2$ is due to magnetic scattering. In the absence of spin, this term is zero, and so is W_1 in Eq. (1.2.14). Obviously, in this situation the relation (1.2.22) cannot be satisfied. A more detailed analysis may be made by considering the contribution to the cross-section of transverse and longitudinal virtual photons seperately. This ratio may be extracted experimentally, and shows that the electrically charged partons have spin-$\frac{1}{2}$. The main results may be understood by remembering that helicity is conserved in electromagnetic interactions (Ex. 2.15). We shall not do this analysis here.

Digression : The Lorentz-invariant form of the double-differential cross-section.

Consider Fig. 1.2 for the reaction

$$e + P \to e' + X .$$

It is convenient to define the variables

$$s = (p + p_e)^2 \quad , \quad t = (p_e - p'_e)^2 = q^2 \quad , \quad u = (p - p'_e)^2 \quad ,$$

where p, p_e and p'_e are the four momenta of the proton, the incoming electron and the scattered electron respectively. Only two of three variables s, t and u are independent, since it is easy to show that

$$s + t + u = (m_e^2 + M_p^2 + m_e^2 + W^2) \quad ,$$

where W is the invariant mass of X, $W^2 = (p_e + p - p'_e)^2$. The double-differential cross-section for the reaction depicted in Fig. 1.2 was given in the labratory frame in Eq. (1.2.14). In the Lorentz-invariant form, it is

$$\left(\frac{d^2\sigma}{dt\,du}\right)_{eP\to eX} = \frac{4\pi\alpha^2}{t^2}\frac{1}{2s^2(s+u)}\left[2xF_1^P(s+u)^2 - 2usF_2^P\right] .$$

Using the Callen-Gross relation (1.2.22), this reduces to

$$\left(\frac{d^2\sigma}{dt\,du}\right)_{eP\to eX} = \frac{4\pi\alpha^2}{t^2}\frac{(s^2+u^2)}{2s^2(s+u)}F_2^P(x) .$$

Here x is defined by Eq. (1.1.3). In this approximation, the cross section is directly proportional to $F_2(x)$. The proton structure function, $F_2^P(x)$, is shown in Fig. 1.12 . The Q^2-dependence is small and has been averaged.

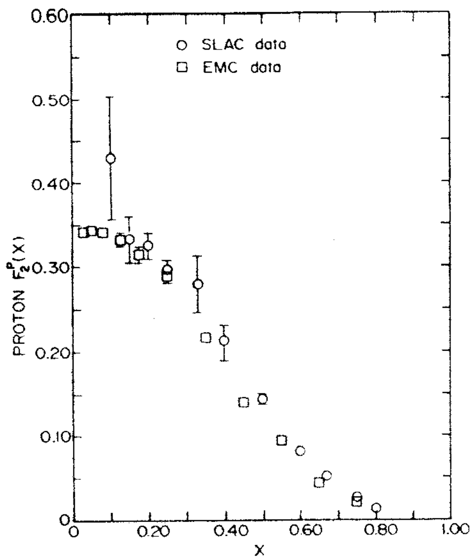

Figure 1.12 The proton structure function, $F_2^P(x)$, averaged over Q^2 from e^-P (SLAC, *Phys. Rev.* **D5**, 528 (1972); **D20**, 1471 (1979)) and μ^-P (EMC, *Nucl. Phys.* **259B**, 189 (1985)) data. In this figure, the EMC data ranged for $Q^2 = 9$–$27\,\mathrm{GeV}^2$, and for beam energy of 120 to 280 GeV. For the SLAC data, the beam energy E_e is in the range 4.5 to 18 GeV, and for $x > 0.4$, $Q^2 = 9$–$12\,\mathrm{GeV}^2$; for smaller x, $Q^2 = 2.5$–$7\,\mathrm{GeV}^2$.

Deep-inelastic scattering data give us the momentum distribution function of the quarks, $f_i(x)$, directly. From the digression above, note that $F_2^N(x)$ may be obtained directly from the double-differential inelastic cross-section. From Eq. (1.2.20), this in turn is related to $f_i(x)$. To illustrate the method, we derive a simple expression for $(F_2^P - F_2^n)$. Consider valence quarks of flavor u, d and s, and $q\bar{q}$ pairs of the same flavors (belonging to the sea) in the nucleon. The distribution function for the u valence quarks in the proton is $f^P_{u_{\text{valence}}}(x)$, which is too cumbersome a notation. Let us, instead, denote this by $u_V^P(x)$. From Eq. (1.2.20), $F_2(x)/x = \sum_i e_i^2 f_i(x)$. This gives,

$$\frac{F_2^P(x)}{x} = \frac{4}{9}u_V^P(x) + \frac{1}{9}d_V^P(x) + \text{Sea contribution}\,. \tag{1.2.23}$$

We assume that the u-quark charge $e_u = \frac{2}{3}$, and for the d-quark $e_d = -\frac{1}{3}$ in units of the proton charge e. There are two valence u quarks and one

valence d-quarks in the pr

$$\int_0^1 u_V^P(x)$$

Similarly, in the neutron,

$$\frac{F_2^n(x)}{x} = \frac{4}{9}u_V^n(x) +$$

with

$$\int_0^1 u_V^n(x)$$

If we further assume that

$$u_V^P($$
$$d_V^P($$

and the sea contributions a

$$[F_2^P(x) -$$

In Fig. 1.10 or 1.11, we the
the distribution of u and d

Exercise 1.3

Make the simplify a
distributions for all flavors
$S(x)$. Show that Eq. (1.2.2

$$\frac{F_2^P(x)}{x} =$$

Experimentally, there is evi
stant as $x \to 0$. What can
observation?

Finally, can we deduce a
through the data? Note, fro

$$\int_0^1 F_2(x$$

valence d-quarks in the proton, giving

$$\int_0^1 u_V^P(x)\,dx = 2 \quad , \quad \int_0^1 d_V^P(x)\,dx = 1 \; .$$

Similarly, in the neutron,

$$\frac{F_2^n(x)}{x} = \frac{4}{9}u_V^n(x) + \frac{1}{9}d_V^n(x) + \text{Sea contribution} \quad , \tag{1.2.24}$$

with

$$\int_0^1 u_V^n(x)\,dx = 1 \quad , \quad \int_0^1 d_V^n(x)\,dx = 2 \; .$$

If we further assume that

$$\begin{aligned} u_V^P(x) &= d_V^n(x) = u_V(x) \\ d_V^P(x) &= u_V^n(x) = d_V(x) \quad , \end{aligned}$$

and the sea contributions are the same, then

$$\left[F_2^P(x) - F_2^n(x)\right] = \tfrac{x}{3}\left[u_V(x) - d_V(x)\right] \; . \tag{1.2.25}$$

In Fig. 1.10 or 1.11, we therefore get a direct measure of the difference in the distribution of u and d valence quarks in the proton.

Exercise 1.3

Make the simplifying assumption that the sea quark and antiquark distributions for all flavors u, d and s are the same, and denote it by $S(x)$. Show that Eq. (1.2.23) is modified to

$$\frac{F_2^P(x)}{x} = \frac{4}{9}u_V^P(x) + \frac{1}{9}d_V^P(x) + \frac{4}{3}S(x) \; .$$

Experimentally, there is evidence that $F_2(x)$ approaches a nonzero constant as $x \to 0$. What can you deduce about the sea-quarks from this observation?

Finally, can we deduce anything about the gluons, at least indirectly, through the data? Note, from Eq. (1.2.20) that

$$\int_0^1 F_2(x)\,dx = \sum_i e_i^2 \int_0^1 dx\, x f_i(x) \; . \tag{1.2.26}$$

In our simplified notation, let us denote by $P_u^{(P)}$ the fraction of the momentum carried by the u quarks in the proton, including the sea contribution, *i.e.*,

$$P_u^{(P)} = \int_0^1 dx\, x\left(u_V^P + u_{\rm sea}^P + \bar{u}_{\rm sea}^P\right) .$$

Then, from Eq. (1.2.26), we get

$$\int_0^1 F_2^P(x)\, dx = \frac{4}{9} P_u^{(P)} + \frac{1}{9} P_d^{(P)} .$$

The quantity P_d is the fractional momentum carried by the d-quarks. Experimentally, one finds that

$$\int_0^1 F_2^{eP}(x)\, dx \approx 0.18 \quad ,$$

$$\int_0^1 F_2^{en}(x)\, dx \approx 0.12 .$$

We then get

$$\frac{4}{9} P_u^{(P)} + \frac{1}{9} P_d^{(P)} \approx 0.18 \quad ,$$

and similarly

$$\frac{4}{9} P_u^{(n)} + \frac{1}{9} P_d^{(n)} \approx 0.12 \quad ,$$

where $P_u^{(n)}$ is the momentum fraction carried by the u-quark in the neutron, *etc.* Making the reasonable assumption that

$$P_u^{(n)} = P_d^{(P)} \quad , \quad P_d^{(n)} = P_u^{(P)} \quad ,$$

we get

$$P_u^{(P)} \approx 0.36 \quad , \quad P_d^{(P)} \approx 0.18 . \tag{1.2.27}$$

This gives the suprising result that only 54 % of the momentum of the nucleon is carried by the quarks (including the sea-quarks). The rest, it is surmised, must be taken up by the gluons, even though they do not interact with the electron.

As mentioned in Section 1.1, neutrinos and antineutrinos are also very useful in these scattering experiments. Note that in a charged weak current interaction, ν_μ can only interact with the d quarks and $\bar{\nu}_\mu$ with the u quarks:

$$\begin{aligned} \nu_\mu + d &\to \mu^- + u \quad , \\ \bar{\nu}_\mu + u &\to \mu^+ + d . \end{aligned} \tag{1.2.28}$$

For a reaction $\nu + N \to \nu'$
cross section is modif
term proportional to
opposite signs for νN and
interesting sum rules that
example, one gets the Bjor

$$\int_0^1$$

Such sum-rules may also b
additional correction terms.
in lowest-order perturbativ
to yield better agreement v

It may not be out of pla
at this point. It refers to the
(European Muon Collabor
scattering, that the bound
is substantially different fr
observed with electron bea
of some old SLAC data[23],
later, on a variety of nuclea
the EMC and SLAC data
Fig. 1.13 . It should be no
the SLAC experiment (upto
energy range 100–300 GeV,
x-values. There has be
nuclear community, and the
experimental results. We w
us too far from the focus of

In this and the preceding
scattering results that have
a nulceon. These experimen
behave as essentially free pa
way for QCD to be taken s
asymptotic freedom (see Sec
about structure functions a
article by West[25] and the sta
shall concentrate on the reso
the deep-inelastic scattering
described in terms of the sin

For a reaction $\nu + N \to \nu' + X$, the expression for the double-differential cross section is modified from expression (1.2.14) by the addition of a term proportional to W_3 with the same angle-dependence as W_1, but has opposite signs for νN and $\bar{\nu} N$. The νN structure functions obeys some interesting sum rules that may be derived easily in the parton model. For example, one gets the Bjorken rule

$$\int_0^1 dx \left[F_1^{\bar{\nu}P} - F_1^{\nu P}\right] = 2 \ . \tag{1.2.29}$$

Such sum-rules may also be derived in large-Q^2 perturbative QCD with additional correction terms. For example, the right-hand side of Eq. (1.2.29) in lowest-order perturbative QCD is $2(1 - 2\alpha_s(Q^2)/3\pi)$, and this is tested to yield better agreement with experiment.

It may not be out of place here to mention the so-called "EMC effect" at this point. It refers to the suprising observation, made first by the EMC (European Muon Collaboration) group[22] in deep inelastic muon-nucleus scattering, that the bound nucleon structure function inside the nucleus is substantially different from that of a free nucleon. The effect was also observed with electron beams at much lower values of Q^2 by a reanalysis of some old SLAC data[23], and by a more detailed SLAC experiment[24] later, on a variety of nuclear targets. There is some disagreement between the EMC and SLAC data for ^{56}Fe at low x ($x < 0.3$). This is shown in Fig. 1.13 . It should be noted that the electron beam energy range in the SLAC experiment (upto $\sim 25\,\mathrm{GeV}$) was very different from the muon energy range 100–300 GeV, and Q^2's were very dissimilar too for the same x-values. There has been a great deal of interest in the EMC-effect in the nuclear community, and there is controversy in the interpretation of the experimental results. We would not enter into such topics that will take us too far from the focus of the present discussion.

In this and the preceding section, We have given a brief account of the scattering results that have led us to believe that quarks do exist inside a nulceon. These experiments also showed that for large-Q^2 the quarks behave as essentially free particles. As mentioned earlier, this paved the way for QCD to be taken seriously, when it was discovered that it has asymptotic freedom (see Section 5.4). The reader who wants to learn more about structure functions and deep inelastic scattering should study the article by West[25] and the standard texts[10]. For the rest of the chapter, we shall concentrate on the resonance excitations of the nucleon (rather than the deep-inelastic scattering) by pions, and how these resonances may be described in terms of the simplest constituent quark model.

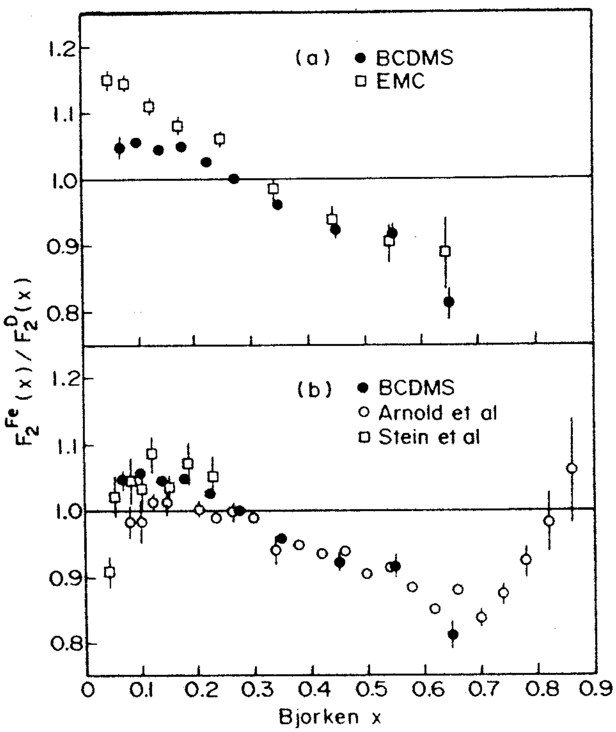

Figure 1.13 The EMC-effect in ^{56}Fe. By taking the ratio of the inclusive inelastic lepton nucleus cross sections, $\left({}^1\!/_A\,\sigma^A / {}^1\!/_2\,\sigma^D\right)$, the ratio of the nucleon structure function, F_2^N, in ^{56}Fe and deuteron is extracted under certain assumptions. This is denoted by $F_2^{\mathrm{Fe}}(x)/F_2^D(x)$ in the figure and plotted against x. The BCDMS muonic data are compared with (a) earlier EMC muonic data, and (b) electron scattering measurements. For details see A. C. Benvenuti *et al.*, (BCDMS collaboration), CERN-EP/87-13. (1987).

1.3 NUCLEON RESONANCES AND BARYON SPECTROSCOPY

A large number of excited states of the nucleon have been identified[26] in the energy range 1 to 3 GeV. These decay strongly to the ground state, and typically have widths in the range 100–300 MeV. Consequently, there is considerable overlapping of the resonances, more so with increasing excitation energy. The quantum numbers of many of the low lying states have

been identified. The spect
give strong indirect e
duce the subject here to p
the particle-data tables[26].
delta, but the pattern of th
These will be of immediate
The nucleon resonances
production and electroprod
charge independent, there a
corresponding to the isospi
the third component I_3. A f
a plot of the total πN cross
$s = (p_\pi + p_N)^2$. But the m
careful partial wave analysi
$\sigma_T(\pi^+ p)$ and $\sigma_T(\pi^- p)$ are
straighforward analysis sho
channel):

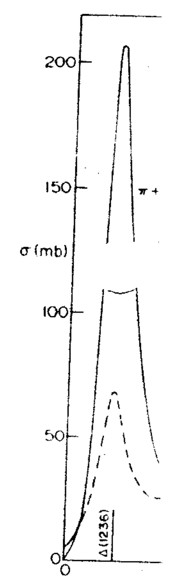

Figure 1.14 A Schematic plo
the pion kinetic energy T_π.

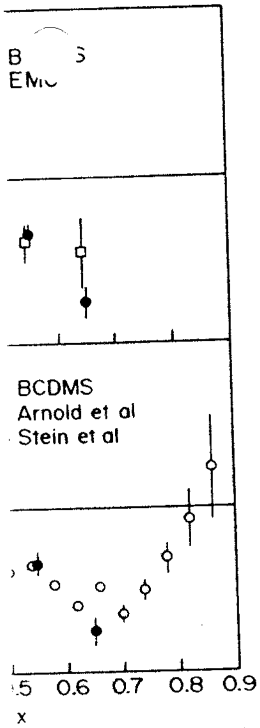

.aking the ratio of the inclusive in- $'/{}^1\!/_2\sigma^D)$, the ratio of the nucleon is extracted under certain assump- ı ' figure and plotted against x. ı (a) earlier EMC muonic data, and letails see A. C. Benvenuti *et al.*, 1987).

5 AND BARYON

ıucleon have been identified[26] in ay strongly to the ground state,)0–300 MeV. Consequently, there ces, more so with increasing exci- nany of the low lying states have

been identified. The spectroscopy of these states (and of other baryons) give strong indirect evidence to the quark degrees-of-freedom. We introduce the subject here to provide some background so the reader may use the particle-data tables[26]. We concentrate mainly on the nucleon and the delta, but the pattern of the data for the other baryons are also presented. These will be of immediate use in the next two sections.

The nucleon resonances are found in πN scattering, and in pion photoproduction and electroproduction experiments. Strong interactions being charge independent, there are only two independent scattering amplitudes corresponding to the isospin channels $I = \frac{3}{2}$ and $I = \frac{1}{2}$, independent of the third component I_3. A few low-lying prominent resonances show up in a plot of the total πN cross section as a function of the energy $\sqrt{s}$, where $s = (p_\pi + p_N)^2$. But the majority of the resonances are found through a careful partial wave analysis of the data. In Fig. 1.14, the cross sections $\sigma_T(\pi^+ p)$ and $\sigma_T(\pi^- p)$ are plotted versus the pion kinetic energy T_π. A straighforward analysis shows[27] that (superscripts specifying the isospin channel):

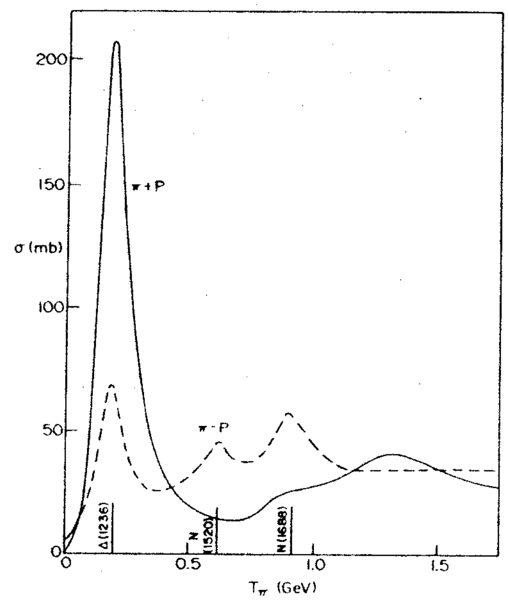

Figure 1.14 A Schematic plot of total $\pi^+ P$ and $\pi^- P$ cross sections against the pion kinetic energy T_π.

$$\sigma_{\mathrm{T}}(\pi^+p) = \sigma_{\mathrm{T}}^{(3/2)} \quad , \quad \sigma_{\mathrm{T}}(\pi^-p) = \tfrac{2}{3}\sigma_{\mathrm{T}}^{(1/2)} + \tfrac{1}{3}\sigma_{\mathrm{T}}^{(3/2)} \,. \tag{1.3.1}$$

The first relation is obvious, while the second requires a little computation involving the Clebsch-Gordon coupling coefficients. Both the plots are dominated by the "delta" resonance, $\Delta(1232)$, which has $I = \frac{3}{2}$ and angular momentum $J = \frac{3}{2}$. Some other peaks may be identified, but the background, and the overlapping of resonances wash out the structure at higher energies.

Exercise 1.4

The elastic scattering amplitude of a spinless particle is

$$f(k,\theta) = \frac{1}{k}\sum_{\ell}(2\ell+1)a_\ell P_\ell(\cos\theta) \quad , \quad \mathbf{k} = \frac{m_2\mathbf{k}_1 - m_1\mathbf{k}_2}{(m_1+m_2)} \,.$$

Here $\mathbf{k}$ is the relative momentum, $k = |\mathbf{k}|$, and θ is the scattering angle. In this partial wave expansion, $a_\ell = (\eta_\ell e^{2i\delta_\ell} - 1)/2i$, where η_ℓ is real $(0 \le \eta_\ell \le 1)$, and is called the inelasticity parameter. The phase shift of the ℓth partial wave is given by the real parameter δ_ℓ. The optical theorem is

$$\sigma_{\mathrm{T}}(k) = \frac{4\pi}{k}\Im m\, f(k,0) \,.$$

If the scattering is dominated by only one partial wave ℓ, then show that

$$\sigma_{\mathrm{T}} \le \frac{4\pi}{k^2}(2\ell+1) \,.$$

In πN scattering, the total angular momentum $J = \ell \pm \frac{1}{2}$. The $J = \frac{3}{2}$ state, for example, may have $\ell = 1$ and $\ell = 2$. Assuming that only one of these channels contrubute to $\Delta(1232)$,

$$\sigma_{\mathrm{T}} \le \frac{2\pi}{k^2}(2J+1) \,.$$

The relative $\mathbf{k}$, as defined above, is independent of the *c.m.* momentum $\mathbf{K} = \mathbf{k}_1 + \mathbf{k}_2$. It is convenient to evaluate $\mathbf{k}$ in the *c.m.* frame, where $\mathbf{K} = 0$. In this frame, $\mathbf{k}_1 = -\mathbf{k}_2 = \mathbf{k}$. One also refers to $\mathbf{k}$ as the *c.m.* momentum. Take $\sigma_{\mathrm{T}} = 190\,\mathrm{mb}$ ($1\,\mathrm{mb} = 10^{-27}\mathrm{cm}^2$) at $\sqrt{s} = 1232\,\mathrm{MeV}$. Evaluate k and show that the unitary limit for σ_{T} is reached at this energy for $J = \frac{3}{2}$.

At low energies, it is a
as k^4, showing that t
$\ell = 1$ P-state. The standa
it is a resonance in the π
spectroscopy, every baryoni
in this manner. For exam
state like $D13(1520)$ would
nominal mass 1520 MeV. T
parity, $J^P = \frac{3}{2}^-$, but the N
As mentioned earlier, t
a careful analysis of the ex
sis. Since the pion has no s
isospin channel may be wri

$f(k^2,\theta) =$

where $\hat{\mathbf{n}} = (\mathbf{k}\times\mathbf{k}')/|\mathbf{k}\times\mathbf{k}'|$.
cleon, and $\mathbf{k},\mathbf{k}'$ are the initia
and θ is the angle between
so that f is a scalar, and n
complex, so that at each ene
One of these may be absorbe
parameters to be determine
These may involve unpolari
cross section and the recoil
larized targets. For an
of $f(k^2,\theta)$, as in Ex. (1.
factor, a unique set of partia
the data alone, no matter h
theoretical constraints of an
partial wave is analysed usin
with Breit-Wigner resonanc
is coupled to energy-depend
Using the theoretical constra
set of amplitudes which fit t
the range $E_\pi = 0.42$ to 2.4
reader should see the papers
and others by the Karlsruhe-
It is customary to display
Argand diagrams. Consider t

$f_\ell(k)$

$$\tfrac{2}{3} \quad) + \tfrac{1}{3}\sigma_T^{(3/2)} \ . \qquad (1.3.1)$$

cond requires a little computa-
ing coefficients. Both the plots
$\Delta(1232)$, which has $I = \frac{3}{2}$ and
eaks may be identified, but the
ances wash out the structure at

---

spinless particle is

$$, \quad \mathbf{k} = \frac{m_2\mathbf{k}_1 - m_1\mathbf{k}_2}{(m_1 + m_2)} \ .$$

<|, and θ is the scattering angle.
$\eta_\ell e^{2i\delta_\ell} - 1)/2i$, where η_ℓ is real
y parameter. The phase shift of
arameter δ_ℓ. The optical theorem

$f(k, 0)$.

e partial wave ℓ, then show that

+

mentum $J = \ell \pm \frac{1}{2}$. The $J = \frac{3}{2}$
$\ell = 2$. Assuming that only one of

$+1)$.

ependent of the *c.m.* momentum
uate $\mathbf{k}$ in the *c.m.* frame, where
One also refers to $\mathbf{k}$ as the *c.m.*
$= 10^{-27}\text{cm}^2$) at $\sqrt{s} = 1232\,\text{MeV}$.
nit for σ_T is reached at this energy

At low energies, it is also found that the π^+p cross section σ_T rises as k^4, showing that the scattering is mostly taking place in the relative $\ell = 1$ P-state. The standard notation for $\Delta(1232)$ is $P33$, denoting that it is a resonance in the πN P-state, with $2I = 3$, $2J = 3$. In baryon spectroscopy, every baryonic state, including the ground-states, is written in this manner. For example, the nucleon ground state is $P11(939)$. A state like $D13(1520)$ would refer to a nucleon ($2I = 1$), with $J = \frac{3}{2}$ and nominal mass 1520 MeV. The state itself would have an intrinsic negative parity, $J^P = \frac{3}{2}^-$, but the $N\pi$ resonance is seen in the $\ell = 2$ partial wave.

As mentioned earlier, the identification of these resonances demands a careful analysis of the experimental data through partial wave analysis. Since the pion has no spin, the scattering amplitude $f(k^2, \theta)$ in each isospin channel may be written as

$$f(k^2, \theta) = g(k^2, \theta) + ih(k^2, \theta)\boldsymbol{\sigma} \cdot \hat{\mathbf{n}} \quad , \qquad (1.3.2)$$

where $\hat{\mathbf{n}} = (\mathbf{k} \times \mathbf{k}')/|\mathbf{k} \times \mathbf{k}'|$. Here $\boldsymbol{\sigma}$ is the Pauli spin operator for the nucleon, and $\mathbf{k}, \mathbf{k}'$ are the initial and final pion three moments in *c.m.* system, and θ is the angle between them. Equation (1.3.2) has been constructed so that f is a scalar, and not a pseudoscalar. The functions g and h are complex, so that at each energy and angle there are four real parameters. One of these may be absorbed in an overall phase factor, leaving three real parameters to be determined by three independent sets of experiments. These may involve unpolarized targets, with measurements of differential cross section and the recoil nucleon polarization, or experiments with polarized targets. For an analysis of the data, a partial wave decomposition of $f(k^2, \theta)$, as in Ex. (1.4) is made. Due to the energy-dependent inelastic factor, a unique set of partial wave parameters cannot be extracted from the data alone, no matter how accurate. It becomes necessary to apply theoretical constraints of analyticity through dispersion relations. Each partial wave is analysed using a smoothly varying background term along with Breit-Wigner resonance terms as required. The elastic πN-channel is coupled to energy-dependent inelastic channels like $\pi\Delta, \rho N, \pi N^*$ *etc.* Using the theoretical constraints, it is then possible to arrive at a unique set of amplitudes which fit the scattering data as a function of energy in the range $E_\pi = 0.42$ to $2.4\,\text{GeV}$ in the laboratory frame. The interested reader should see the papers of Cutkosky[28] *et al.* of the CMU-LBL group, and others by the Karlsruhe-Helsinki[29] group.

It is customary to display the πN-elastic scattering amplitudes through Argand diagrams. Consider the partial wave amplitude

$$f_\ell(k) = (\eta_\ell e^{2i\delta_\ell} - 1)/2ik \ . \qquad (1.3.3)$$

We see that

$$\Re e\, k f_\ell(k) = \frac{1}{2}\eta_\ell \sin 2\delta_\ell \quad , \quad \Im m\, k f_\ell(k) = (1 - \eta_\ell \cos 2\delta_\ell)/2 \, . \qquad (1.3.4)$$

One plots an Argand diagram with $2\Im m(kf_\ell)$ along the y-axis and $2\Re e(kf_\ell)$ along the x-axis for various values of k at regular intervals. In the idealized case of no inelasticity ($\eta_\ell = 1$) and a single resonance, the Argand diagram would be a perfect circle with unit radius, the centre on the imaginary axis at i (see Fig 1.15).

Note that at a resonance, $\delta_\ell = \frac{\pi}{2}$, and this correponds to the highest point of the circle. With increasing k, the circle is traced in the anti-clockwise direction, with the "speed" determined by the rate of rise of $\delta_\ell(k)$ with k. In practice, because the inelasticity factor η_ℓ is energy dependent and less than one, the shape of the circle is distorted, and the position of a resonance may be tilted off the imaginary axis. The same diagram often shows more than one resonance. Due to the distortion of the Argand circle and huge background in some cases, it is hard to identify a resonance. Often the speed of the trajectory (the k-values in the plot are at 50 MeV intervals) near a "wiggle" may be the factor in unravelling the

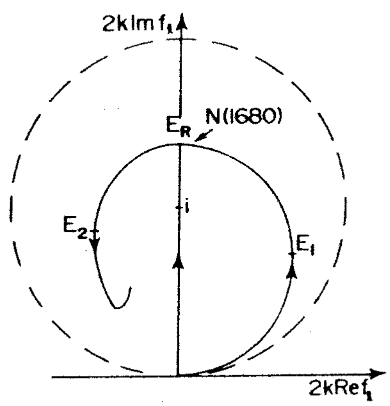

Figure 1.15 An Argand diagram for the πN scattering amplitude in a given partial wave. The dashed plot of the circle is an idealized case for a resonance with no inelastic channels open. The solid curve is a schematic drawing for the πN-scattering amplitude F_{15}. There is a hint of another resonance contributing at the tip of the turning tail.

structure of the partia
ples in the partic- da
resonances are g.
Δ, and for completeı
that contain one or
strangeness quantum
ing to $SU(3)$-flavor an
of these states would
tion of three valence
is eliminated. This w
multiplet-$SU(3)$ nota

Exercise 1.5

Consider the pion
nucleon in a localized
wave function $\sim \sin(k$
states in the presence
a large sphere of radiu
vanishes at $r = R$. Sh

g_ℓ

Here $g_\ell(k)\,dk$ is the n
tween k and $k + dk$,
absence of the interact
over a narrow ran of
in the density of s e
bumps are the resonan
spike of a bound-state

We may have giv
nucleon are seen as re
of the excited states t
decouple from the πN
quark coupling promo
excited states of a baı
examples will be seen
from the πN-channel.
of such states may st
photon has special aff

structure of the partial wave. The reader should look up many such examples in the particle-data tables[26], where a complete list of the established resonances are given. In Table 1.1, we display the resonances of N and Δ, and for completeness also show the excited states of other baryons that contain one or more strange quarks. The strange quark carries a strangeness quantum number $S = -1$. The states are classified according to $SU(3)$-flavor and $SU(6)$ spin$\times$flavor representations. The counting of these states would show that these could be generated by the motion of three valence quarks when the spurious centre of mass motion is eliminated. This would be done in the next two sections, where the multiplet-$SU(3)$ notation will also be explained.

Exercise 1.5

Consider the pion momentum $\mathbf{k}$ in the $c.m.$ frame. It interacts with the nucleon in a localized region, and in elastic scattering has an asymptotic wave function $\sim \sin\left(kr - \frac{\ell\pi}{2} + \delta_\ell\right)$ for large r. To compute the density of states in the presence of the interaction, enclose the system artificially in a large sphere of radius R, imposing the condition that the wave function vanishes at $r = R$. Show that

$$g_\ell(k) - g_\ell^0(k) = \frac{(2\ell+1)}{\pi}\frac{\partial\delta_\ell(k)}{\partial k} .$$

Here $g_\ell(k)\,dk$ is the number of states of a given partial wave ℓ lying between k and $k + dk$, and $g_\ell^{(0)}(k)\,dk$ is the corresponding number in the absence of the interaction. The above formula shows that if δ_ℓ rises steeply over a narrow range of k and then flattens, it will give rise to a sharp bump in the density of states. The elastic width is determined by $\partial\delta_\ell/\partial k$. These bumps are the resonances in the continuum, as opposed to a delta-function spike of a bound-state.

We may have given the impression that all the excited states of a nucleon are seen as resonances in πN scattering. This is not so and some of the excited states that are predicted by the quark model may nearly decouple from the πN channel[30]. In the simple quark model, the pion-quark coupling promotes a single quark from the ground state, but some excited states of a baryon may dominantly be 2-quark excitations. Such examples will be seen in Section 1.5, and such states would decouple from the πN-channel. However, electroproduction and photoproduction of such states may still be possible. In Chapter 7 we shall see that a photon has special affinity to a ρ-meson. In particular, a virtual photon

Table 1.1 Baryons and Their Resonances with (u, d, s) Valence Quarks

$SU(6)$ Reprn.	$SU(3)_f$ Reprn.	J^P	$S = 0$	$S = -1$, $I = 0$	$S = -1$, $I = 1$	$S = -2$	$S = -3$
$56^+(L = 0)$	$^2 8$	$\frac{1}{2}^+$	$N(939)$	$\Lambda(1116)$	$\Sigma(1193)$	$\Xi(1318)$	
$N = 0$	$^4 10$	$\frac{3}{2}^+$	$\Delta(1232)$		$\Sigma(1385)$	$\Xi(1533)$	$\Omega(1672)$
$70^-(L = 1)$	$^2 8$	$\frac{3}{2}^-$	$N(1520)$	$\Lambda(1690)$	$\Sigma(1580)^{**}$	$\Xi(1820)?$	
$N = 1$		$\frac{1}{2}^-$	$N(1535)$	$\Lambda(1670)$	$\Sigma(1620)^{**}$		
	$^4 8$	$\frac{1}{2}^-$	$N(1650)$	$\Lambda(1800)$	$\Sigma(1750)$		
		$\frac{5}{2}^-$	$N(1675)$	$\Lambda(1830)$	$\Sigma(1775)$		
		$\frac{3}{2}^-$	$N(1700)$	?	$\Sigma(1670)$		
	$^2 10$	$\frac{1}{2}^-$	$\Delta(1620)$				
		$\frac{3}{2}^-$	$\Delta(1700)$				
	$^2 1$	$\frac{1}{2}^-$		$\Lambda(1405)$			
		$\frac{3}{2}^-$		$\Lambda(1520)$			
$56^+(L = 0')$	$^2 8$	$\frac{1}{2}^+$	$N(1440)$	$\Lambda(1600)$	$\Sigma(1660)$		
$N = 2$	$^4 10$	$\frac{3}{2}^+$	$\Delta(1600)^{**}$		$\Sigma(1690)^{**}?$		
$56^+(L = 2)$	$^2 8$	$\frac{3}{2}^+$	$N(1720)$	$\Lambda(1890)$	?		
$N = 2$		$\frac{5}{2}^+$	$N(1680)$	$\Lambda(1820)$	$\Sigma(1915)$		
	$^4 10$	$\frac{1}{2}^+$	$\Delta(1910)$				
		$\frac{3}{2}^+$	$\Delta(1920)$		$\Sigma(2080)^{**}$		
		$\frac{5}{2}^+$	$\Delta(1905)$				
		$\frac{7}{2}^+$	$\Delta(1950)$		$\Sigma(2030)$		
$56^+(L = 4)$	$^2 8$	$\frac{7}{2}^+$					
		$\frac{9}{2}^+$	$N(2220)$				
	$^4 10$	$\frac{5}{2}^+$					
		$\frac{7}{2}^+$					
		$\frac{9}{2}^+$	$\Delta(2300)^{**}$				
		$\frac{11}{2}^+$	$\Delta(2420)$				
$70^+(L = 0')$	$^2 8$	$\frac{1}{2}^+$	$N(1710)$	$\Lambda(1800)$	$\Sigma(1880)^{**}$		
$N = 2$	$^4 8$	$\frac{3}{2}^+$	$N(1540)^{*}?$				
	$^2 10$	$\frac{1}{2}^+$	$\Delta(1550)^{*}?$				
	$^2 1$	$\frac{1}{2}^+$	$N(2100)^{*}?$				
$70^+(L = 2)$	$^2 8$	$\frac{5}{2}^+$		$\Lambda(2110)$			
	$^4 8$	$\frac{7}{2}^+$	$N(1990)^{**}?$				
$56^-?$	$^2 8$	$\frac{1}{2}^-$	$N(2090)^{*}?$				
$(L = 1)$		$\frac{3}{2}^-$	$N(2080)^{**}?$				
$N = 3$	$^4 10$	$\frac{1}{2}^-$	$\Delta(1900)$				
		$\frac{3}{2}^-$	$\Delta(1940)^{*}?$		$\Sigma(1940)$		
		$\frac{5}{2}^-$	$\Delta(1930)$				

The two- and one-star states are not confirmed[26].

transforms to a ρ bef
dominance mode[1] S
by the emission a
ω-coupling, so react
states that were mis
production process
Consider first re
along the z-directio
The circularly polari

$$\epsilon^{(+)} =$$

Writing these in
$\epsilon^{(+)} \propto \sin\theta e^{i\phi}, \epsilon^{(-)}$
photon make its wa
bination thereof), a
energy photon may
licity (or the project
only be ± 1. Thus, th
(which has a branc
photon to carry two
ity may only chang
states of $N(940)$ m
$N(1680)\frac{5}{2}^+$, and no
may connect to m_J
$(\frac{3}{2} \to \frac{1}{2})$ ampli
real photons, there
with $J \geq \frac{3}{2}$, and sin
real, being the ma
action $j_\mu A^\mu$ (see C
The helicity amplit
the particle data ta
the nucleon. In pa
amplitudes for the
determine the elect
amplitudes, the for
the shell-model qu
the πN partial wa
three valence quark
for both $N(940)$ an

transforms to a ρ before coupling to a hadron in a model called the vector-dominance model. Such a process may excite states that decay strongly by the emission of a ρ (correlated 2π). This is also true for the isoscalar ω-coupling, so reactions like $\gamma N \to 2\pi N, \gamma N \to 3\pi N$ may unravel those states that were missing in the πN-channel. Besides these, the single pion production process $\gamma N \to \pi N$ has also been studied in great detail[31].

Consider first real photons for simplicity. A real photon propagating along the z-direction has only transverse polarization vector ϵ_x and ϵ_y. The circularly polarized vector are

$$\epsilon^{(+)} = \frac{1}{\sqrt{2}}(\epsilon_x + i\epsilon_y) \quad , \quad \epsilon^{(-)} = \frac{1}{\sqrt{2}}(\epsilon_x - i\epsilon_y) \ .$$

Writing these in spherical polar coordinates, it is at once seen that $\epsilon^{(+)} \propto \sin\theta e^{i\phi}, \epsilon^{(-)} \propto \sin\theta e^{-i\phi}$. Thus the polarization vectors of a real photon make its wave function go like $Y_1^{m=1}$ and $Y_1^{m=-1}$ (or a linear combination thereof), and the $m = 0$ component is absent. Although a high energy photon may carry away many units of angular momentum, the helicity (or the projection of the spin along the direction of propagation) may only be ± 1. Thus, the decay of the resonance $N(1680)\frac{5}{2}^+ \to N(940)\frac{1}{2}^+ + \gamma$ (which has a branching ratio of about 0.3 % for the proton) causes the photon to carry two units of angular momentum ($\Delta J = 2$), but the helicity may only change by one unit ($\Delta m_J = \pm 1$). Therefore, the $m_J = \pm\frac{1}{2}$ states of $N(940)$ may only be connected to the $m_J = \frac{3}{2}$ or $\frac{1}{2}$ states of $N(1680)\frac{5}{2}^+$, and not to the $m_J = \frac{5}{2}$ state. Of course, the $m_J = -\frac{3}{2}$ state may connect to $m_J = -\frac{1}{2}$ of $N(940)$, but this amplitude is related to the $(\frac{3}{2} \to \frac{1}{2})$ amplitude by time-reversal. Thus for proton target coupling to real photons, there are two such amplitudes $A_{3/2}^{(p)}$ and $A_{1/2}^{(p)}$ for resonances with $J \geq \frac{3}{2}$, and similarly two more for a neutron. These amplitudes are real, being the matrix-elements of the hermitian electromagnetic interaction $j_\mu A^\mu$ (see Chapter 5) between the nucleon and the excited state. The helicity amplitudes $A_{3/2}$ and $A_{1/2}$ are listed for many resonances in the particle data tables[26], and constitute a sensitive check to models of the nucleon. In particular, there is considerable interest in the helicity amplitudes for the transitions[32–34] $\Delta(1232) \to N(940) + \gamma$, since these determine the electric quadrupole $E2$ and magnetic dipole $M1$ transition amplitudes, the former depending sensitively on the D-state percentage in the shell-model quark wave function. (This should not be confused with the πN partial wave.) In the simplest version of the quark model, the three valence quarks move in the lowest S-state of the confining potential for both $N(940)$ and $\Delta(1232)$. In such a model the transition $\Delta \to N + \gamma$

is pure $M1$, *i.e.*, a spin flip of a quark from the aligned $J = \frac{3}{2}$ Δ-state to $J = \frac{1}{2}$ state of the nucleon. Deviations from zero in the $E2/M1$ ratio of the amplitudes yield important clues about the structure[34]. This ratio, from analysis of the experimental data is

$$\begin{aligned} E2/M1 = &= -0.013 \pm 0.005^{(26)} \quad , \\ &= -0.015 \pm 0.002^{(34)} \ . \end{aligned} \tag{1.3.5}$$

In the calculation of the electric quadrupole transition matrix-elements using the quark model wave functions, one should be wary of the truncation effects in the basis[35]. One can calculate this matrix-element either through the charge operator ρ or vector-current $\mathbf{j}$, since the two are related through current conservation $\partial_\mu j^\mu = 0$. The two schemes do not yield the same result in a truncated space. Similar ambiguities[36] have been pointed out for the virtual photon process (through electroproduction) $\gamma + N \to \Delta$, where the helicity zero longitudinal and scalar amplitudes contribute, and are again related through current conservation. Such problems also arise in nuclear physics[37].

As mentioned already, in the electroproduction of resonances a virtual photon absorption is involved,and helicity zero is also allowed. The Q^2-dependence of the helicity amplitudes, including $A_{1/2}$ and $A_{3/2}$, have been extracted for various resonances through (e, e') experiments. The electric and magnetic transition form factors $G_E(Q^2)$ and $G_M(Q^2)$ may be expressed in terms of $A_{1/2}(Q^2)$ and $A_{3/2}(Q^2)$. These data pose the severest tests to models of the nucleon. The reader should look up ref. 38 for more details.

1.4 THE COUNTING OF STATES AND SYMMETRY

The large number of baryonic states diplayed in Table 1.1 (and others not detected experimentally) may be shown to arise from the motion of three confined valence quarks, interacting with spin-dependent forces. The valence quarks carry the quantum numbers of the baryonic state. In the low-lying spectra, there is no direct evidence of explicit gluonic degrees of freedom, although QCD predictions call for "glue-ball" states (with no valence quarks) in the GeV mass range (see Ex. 3.5 for details). It is possible that such states mix appreciably with some of the conventional mesonic $q\bar{q}$ states, and experimental detection is difficult.In this section, we shall only consider the valence quarks, and figure out, purely from symmetry considerations, how many low-lying odd and even parity excitations of a baryon may be expected. This may be done through the properties of group representation, but we shall do the counting by elementary methods[39], and later introduce the group theoretical language (see Appendix D).

In nuclear physics,the proton and the neutron may be considered to be identical particles when the isospin quantum numbers are introduced. Similarly, for the counting of states, the light quarks u, d and s may be treated on an equal footing, but having different "flavors". The quantum numbers carried by the light quarks are shown in Table 1.2 . The "mass" of the s-quark is considerably larger than u and d, so the flavor symmetry is broken appreciably. This removes the the mass-degeneracy in a mulitplet, but the counting is not affected. In the three-quark system, the total wave function must be antisymmetric with respect to the interchange of a pair of quarks. The wave function has space, spin, flavor and color degrees of freedom. The latter may be viewed as a strong "charge" that gauge couples to the gluons[40] to generate strong interactions (see Chapter 5). A quark of a given flavor has one of three possible colors. This allows, for example, Δ^{++} to be constituted from uuu, each u having a different color but all other quantum numbers the same. Since the long-range force between color charges must keep increasing to account for the confinement of quarks and gluons in a hadron, and there is no such long-range force between hadrons, a hadron must be color neutral. In a meson ($q\bar{q}$) or a baryon (qqq), the wave function containing the color degrees of freedom seperates out from the rest[41]. In a baryon, the color singlet wave function is a (3×3) determinant, antisymmetric under the exchange of a pair. This in turn means that the rest of the wave function, containing the space, spin and flavor coordinates, be symmetric. We now classify the permutation symmetry of the states keeping the above restriction in mind, starting with the spin degree of freedom.

Table 1.2 The Quantum Numbers Carried by the Light Quarks

Flavor	u	d	s
Charge	$\frac{2}{3}$	$-\frac{1}{3}$	$-\frac{1}{3}$
Isospin I	$\frac{1}{2}$	$\frac{1}{2}$	0
I_3	$\frac{1}{2}$	$-\frac{1}{2}$	0
Strangeness	0	0	-1
Baryon Number	$\frac{1}{3}$	$\frac{1}{3}$	$\frac{1}{3}$

Spin

Three spin-$\frac{1}{2}$ quarks may give rise to a total spin $S = \frac{3}{2}$ or $S = \frac{1}{2}$. The $S = \frac{3}{2}$ states are four in number (corresponding to $S_z = \frac{3}{2}, \frac{1}{2}, -\frac{1}{2}$ and $-\frac{3}{2}$). and are symmetric under the interchange of any two spins. For example, the $S = \frac{3}{2}, S_z = \frac{3}{2}$ state is

$$\chi^S_{\frac{3}{2},\frac{3}{2}} = \alpha(1)\alpha(2)\alpha(3) \quad , \tag{1.4.1}$$

where $\alpha(1)$ is the spin-up Pauli spinor for particle 1 (we are using the nonrelativistic formalism). The superscript S (for symmetric) on the spin function χ denotes the permutation symmetry of the state. In addition, there are two types of mixed symmetric states, $\chi^\rho_{1/2}$ and $\chi^\lambda_{1/2}$ (we suppress the S_z-quantum number of simplicity) with total spin $S = \frac{1}{2}$. χ^ρ is formed by combining the spins of 1 and 2 to form $S_{12} = 0$, and then coupling to the spin S_3 (of the third particle) to yield $S = \frac{1}{2}$, *i.e.*, $(S_{12} = 0 \otimes S_3 = \frac{1}{2}) \Rightarrow S = \frac{1}{2}$. The wave function

$$\chi^\rho_{\frac{1}{2},\frac{1}{2}} = \frac{1}{\sqrt{2}}\big(\alpha(1)\beta(2) - \beta(1)\alpha(2)\big)\alpha(3) \quad , \tag{1.4.2}$$

is antisymmetric between particles 1 and 2, but there is no overall symmetry under the exchange $1 \leftrightarrow 3$ or $2 \leftrightarrow 3$. A mixed-symmetric wave function, with antisymmetry between $1 \leftrightarrow 2$ will be labelled by the superscript ρ. Obviously, there are two distinct ρ-type states corresponding to $S_z = \frac{1}{2}$ and $S_z = -\frac{1}{2}$. The λ-type mixed symmetric state, $\chi^\lambda_{1/2}$, is constructed by coupling spins of particles 1 and 2 to 1, and then coupling spin S_3 to yield $\frac{1}{2}$: $(S_{12} = 1 \otimes S_3 = \frac{1}{2}) \Rightarrow S = \frac{1}{2}$. The wave function, in obvious notation, is

$$\chi^\lambda_{1/2,1/2} = \sum_{m_s} (1\ \tfrac{1}{2}\ m\ m_s|\tfrac{1}{2}\ \tfrac{1}{2})|1\ m\rangle|\tfrac{1}{2}\ m_s\rangle \quad ,$$

where the Clebsch-Gordon coefficients are listed in the Particle-data table. We get

$$\begin{aligned}\chi^\lambda_{1/2 1/2} &= \sqrt{\frac{2}{3}}|1\ 1\rangle|\tfrac{1}{2}\ -\tfrac{1}{2}\rangle - \sqrt{\frac{1}{3}}|1\ 0\rangle|\tfrac{1}{2}\ \tfrac{1}{2}\rangle \quad , \\ &= \frac{1}{\sqrt{6}}(2\alpha\alpha\beta - \alpha\beta\alpha - \beta\alpha\alpha) \quad ,\end{aligned} \tag{1.4.3}$$

where $\alpha\alpha\beta$ is a sho
antisymmetric s s
write

Since each quark can
quark system. The re
metric, and the rest
the three quarks on
out by first coupling
an alternate, but not

Exercise 1.6

Check that

$\chi^\lambda_{1/2}$

Also find $\chi^S_{3/2,1/2}, \chi^S_{3/2,}$

Flavor

Consider again three
flavors, u, d, or s. e
accordingly to their s
2 and 3, are denoted
three flavors u, d, s, w
for the quarks 2 and
Clearly, we may have
the second and third
states in which two of
Clearly, there are six
each symmetrized in
from the combination

$\phi^S = [u(1)d($

al n $S = \frac{3}{2}$ or $S = \frac{1}{2}$. The
ing to $S_z = \frac{3}{2}, \frac{1}{2}, -\frac{1}{2}$ and $-\frac{3}{2}$).
f any two spins. For example,

3) , (1.4.1)

particle 1 (we are using the
S (for symmetric) on the spin
ietry of the state. In addition,
tes, $\chi^\rho_{1/2}$ and $\chi^\lambda_{1/2}$ (we suppress
total spin $S = \frac{1}{2}$. χ^ρ is formed
$S_{12} = 0$, and then coupling to
$S = \frac{1}{2}$, *i.e.*, ($S_{12} = 0 \otimes S_3 =$

1)$\alpha(2))\alpha(3)$, (1.4.2)

2, but there is no overall sym-
$\to$ 3. A mixed-symmetric wave
$\to$ 2 will be labelled by the su-
nct ρ-type states corresponding
d symmetric state, $\chi^\lambda_{1/2}$, is con-
2 to 1, and then coupling
$S = \frac{1}{2}$. The wave function, in

$\frac{1}{2})|1\ m\rangle|\frac{1}{2}\ m_s\rangle$,

listed in the Particle-data table.

$\sqrt{\frac{1}{3}}|1\ 0\rangle|\frac{1}{2}\ \frac{1}{2}\rangle$,

$- \beta\alpha\alpha)$, (1.4.3)

where $\alpha\alpha\beta$ is a short-hand for $\alpha(1)\alpha(2)\beta(3)$, *etc.* Note that no totally antisymmetric spin-state is possible for the 3-q system. In short, we may write

$$2^3 = 8 = \underbrace{4}_{S} + \underbrace{2}_{\rho} + \underbrace{2}_{\lambda} \ . \tag{1.4.4}$$

Since each quark can be spin up or down, there are 2^3 states in a three-quark system. The relation (1.4.4) implies that 4 of these states are symmetric, and the rest mixed symmetric. Note that since we are treating the three quarks on an equal footing, the same analysis could be carried out by first coupling 2 and 3 to S_{23} *etc.* The basis generated thereby is an alternate, but not an independent one from the earlier construct.

Exercise 1.6

Check that

$$\chi^\lambda_{1/2\,-1/2} = -\frac{1}{\sqrt{6}}(2\beta\overset{\beta}{\cancel{\alpha}}\alpha - \beta\alpha\beta - \alpha\beta\beta) \ .$$

Also find $\chi^S_{3/2,1/2}, \chi^S_{3/2,-1/2}$.

Flavor

Consider again three quarks, each of which may have one of the three flavors, u, d, or s. There are, in this case, $3^3 = 27$ states. To classify them accordingly to their symmetry, consider Fig. 1.16 . The three quarks, 1, 2 and 3, are denoted by the three crosses. Quark 1 may have any of the three flavors u, d, s, which are arranged under 1 in a column. Similarly for the quarks 2 and 3. How many symmetric states can be constructed? Clearly, we may have states like $u(1)u(2)u(3)$, and two more like this from the second and third row of Fig. 1.16 . We may also construct symmetric states in which two of the quarks have the same flavor, and one different. Clearly, there are six such combinations udd, uss, duu, dss, suu and sdd, each symmetrized in 1, 2, and 3. For example, one such symmetric state from the combination udd is

$$\phi^S = \left[u(1)d(2)d(3) + d(1)u(2)d(3) + d(1)d(2)u(3)\right]/\sqrt{3} \ .$$

1	2	3
X	X	X
u	d	s
u	d	s
u	d	s

Figure 1.16 Construction of the flavor wave function. The three quarks are denoted by crosses and numbered. Each quark may have flavors u, d or s, as shown in a column under it. (Our treatment closely follows the article by Feynman[39]).

Furthermore, there is one symmetric combination of the type uds, where all three flavors are different. Thus there are in all 10 states of the symmetric type. Also, since we are considering three quarks and three flavors, there is only one determinantal combination which is totally antisymmetric under the exchange of any pair. The rest of the sixteen states must be of the mixed symmetric type. Of these, 8 are of ρ-type (antisymmetric in 1 and 2), and 8 λ-type (symmetric in 1 and 2). We may the write

$$3^3 = 27 = \underbrace{10}_{S} + \underbrace{8}_{\rho} + \underbrace{8}_{\lambda} + \underbrace{1}_{A} \ . \tag{1.4.5}$$

For the N and Δ states (the nonstrange sector), only the u and d quarks are involved, and the flavor wave functions are constructed to form states of good isospin $I = \frac{1}{2}$ and $I = \frac{3}{2}$. These may be formed in exactly the same way as the spin functions with $S = \frac{3}{2}$ and $S = \frac{1}{2}$. For example,

$$\phi^S_{\Delta^{++}} = u\,u\,u \quad , \quad \phi^\rho_p = \frac{1}{\sqrt{2}}(ud - du)u \quad ,$$
$$\phi^\lambda_p = \frac{1}{\sqrt{6}}(2uud - udu - duu) \ , \ \phi^\lambda_n = -\frac{1}{\sqrt{6}}(2ddu - dud - udd) \ . \tag{1.4.6}$$

Spin×Flavor Wave Functions

It is now easy to classify the combined spin flavor ($2^3 \times 3^3 = (6)^3 = 216$) states according to their permutation symmetry. In group theory language, we have already seen the multiplet structure of the states in $SU(2)_{\text{spin}}$ and $SU(3)_{\text{flavor}}$ and now we are about to combine these to form the $SU(6)$ multiplets[42]. From Eqs. (1.4.4) and (1.4.5), we may combine the 4 symmetric spin states with the 10 symmetric flavor states to obtain 40 states which are symmetric in the Hilbert space of spin and flavor. These are denoted by ${}^4 10$, the 4 corresponding to the $(2S+1)$ spin states with $S = \frac{3}{2}$. Similarly, the mixed symmetric spin states may be combined with the mixed symmetric flavor states to yield other symmetric combinations with $S = \frac{1}{2}$. The combination that is symmetric under exchange of any pair is $(\chi^\rho \phi^\rho + \chi^\lambda \phi^\lambda)$. Such combinations yield 2×8 symmetric states, and are denoted by ${}^2 8$. We may now write

$$ {}^4 10 + {}^2 8 = 56\,(S) \,. \tag{1.4.7} $$

Referring to Table 1.1, we note that the ground state spin-$\frac{1}{2}$ octet, ${}^2 8$, and the spin-$\frac{3}{2}$ decuplet, ${}^4 10$, form these set of 56 states. If there were no spin-dependent forces between the quarks, one would expect no mass difference between the ${}^2 8$ and the ${}^4 10$ multiplets. We see from Table 1.1 that this is not so, the baryons with $S = \frac{3}{2}$ are consistently heavier. Even within the members of a flavor multiplet (like ${}^2 8$), there is a considerable mass splitting, reflecting the heavier mass of the strange quark.

The mixed symmetric spin and flavor states may also be combined to form antisymmetric combinations under the exhange of any pair. Such an antisymmetric form, also denoted by ${}^2 8$, is $(\chi^\rho \phi^\lambda - \chi^\lambda \phi^\rho)$. Another antisymmetric form, ${}^4 1$, is obtained by combining the antisymmetric flavor part with the symmetric spin functions. In total, there are

$$ {}^4 1 + {}^2 8 = 20\,(A) \quad , \tag{1.4.8} $$

antisymmetric spin-flavor states. There is no firm experimental evidence for such states.

Out of the $3^3 \times 2^3 = 216$ states, we have arranged 56 as symmetric and 20 as antisymmetric. The rest of the 140 states are mixed symmetric, split equally in ρ- and λ-types. In obvious notation, we have

$$ \begin{aligned} & {}^2 10 + {}^4 8 + {}^2 8 + {}^2 1 = 70\,(\rho) \\ \text{and} \qquad & {}^2 10 + {}^4 8 + {}^2 8 + {}^2 1 = 70\,(\lambda)\,. \end{aligned} \tag{1.4.9} $$

Table 1.3 Spin-flavor Wave Functions of a Baryon Classified According to Permutation Symmetry*

56 (S)	
^{410} : $\chi^S\phi^S$	^{28} : $(\chi^\rho\phi^\rho + \chi^\lambda\phi^\lambda)/\sqrt{2}$
20 (A)	
^{41} : $\chi^S\phi^A$	^{28} : $(\chi^\rho\phi^\lambda - \chi^\lambda\phi^\rho)/\sqrt{2}$
70 (ρ)	
^{210} : $\chi^\rho\phi^S$	^{48} : $\chi^S\phi^\rho$
^{28} : $(\chi^\rho\phi^\lambda + \chi^\lambda\phi^\rho)/\sqrt{2}$	^{21} : $\chi^\rho\phi^A$
70 (λ)	
^{210} : $\chi^\lambda\phi^S$	^{48} : $\chi^S\phi^\lambda$
^{28} : $(\chi^\rho\phi^\rho - \chi^\lambda\phi^\lambda)/\sqrt{2}$	^{21} : $\chi^\lambda\phi^A$

* The spin wave functions χ^S, χ^ρ and χ^λ are defined in Eqs. (1.4.1–1.4.3) for maximum S_z. The flavor wave functions ϕ in the nonstrange sector are given by Eq. (1.4.6). The antisymmetric ϕ^A is a detrimental state in u, d, s.

The wave function for the ^{28} ρ-type state is $(\chi^\rho\phi^\lambda + \chi^\lambda\phi^\rho)$, whereas for the ^{28} λ-type state is $(\chi^\rho\phi^\rho - \chi^\lambda\phi^\lambda)$. In Table 1.1, the odd-parity excitations (under 70^-) fall in this category. We shall soon see how the spin-flavor states are combined with the wave function of the spatial part to construct totally symmetric states. In Table 1.3, we list, for completeness, the spin-flavor wave functions of various permutation symmetries.

1.5 THE CONSTITUENT QUARK MODEL IN THE OSCILLATOR BASIS

To count the states of a baryon allowed by symmetry considerations, we now have to construct the spatial states and combine these appropriately with the spin-flavor wave functions of the last section. For this purpose it is most convenient to use the nonrelativistic oscillator model, that was developed more than twenty years back[43,44]. Much later, it was pointed out by De Rújula *et al.*[45] that the spin-dependent hyperfine potential between two quarks due to one-gluon exchange explains the mass splittings between the ^{28} and ^{410} members of the ground state baryons. Isgur and

Karl[46] used the basi
ize the hyperfine c
a highly sucessfu
clear why a nonrelati
eral grounds the moti
mass m, localized in
the uncertainty relati
the constituent quark
the u, d and s flavore
and note a point in th
of the centre-of-mass
tic framework. This i
the excited states. In
done analytically. Th

$$\mathcal{H}_0 = \frac{1}{2m}(\mathbf{p}_1^2$$

Here quarks 1 and 2
3 has mass m'. The
ignored. For N and
are confined in an osc
flavor quantum numb
the *c.m.* variables:

$$\boldsymbol{\rho} = \frac{(\mathbf{r}_1 - \mathbf{r}_2)}{\sqrt{2}} \quad \boldsymbol{\lambda} =$$

Note that the coordin
exchange of $\mathbf{r}_1$ and $\mathbf{r}_2$.
wavefunctions. Define

$$M = 2m + m'$$

and the momenta conj

$$\mathbf{p}_\rho = m_\rho\dot{\boldsymbol{\rho}}$$

It is straightforward to

$$\mathcal{H}_0 = \left(\frac{p_\rho^2}{2m_\rho} + \right.$$

s of a Baryon
ı Symmetry*

$(\chi^\rho\phi^\rho + \chi^\lambda\phi^\lambda)/\sqrt{2}$
$(\chi^\rho\phi^\lambda - \chi^\lambda\phi^\rho)/\sqrt{2}$
$\chi^S\phi^\rho$ $\chi^\rho\phi^A$
$\chi^S\phi^\lambda$ $\chi^\lambda\phi^A$

$^\lambda$ are defined in Eqs. (1.4.1–
unctions ϕ in the nonstrange
ymmetric ϕ^A is a detrimental

tate is $(\chi^\rho\phi^\lambda + \chi^\lambda\phi^\rho)$, whereas
. In Table 1.1, the odd-parity
ory. We shall soon see how the
ave function of the spatial part
T 1.3, we list, for complete-
ious permutation symmetries.

RK MODEL IN THE

y symmetry considerations, we
nd combine these appropriately
e last section. For this purpose
vistic oscillator model, that was
3,44. Much later, it was pointed
pendent hyperfine potential be-
nge explains the mass splittings
ground state baryons. Isgur and

Karl[46] used the basis generated by the oscillator potential to diagonalize the hyperfine and the tensor one-gluon exchange potentials. This is a highly sucessful model in spectroscopy and baryon structure. It is not clear why a nonrelativistic model should be so good since on rather general grounds the motion of light quarks should be relativistic. A particle of mass m, localized in a volume of radius R, has momentum $\sim 1/R$ through the uncertainty relation. Its kinetic energy $\langle T\rangle \ll m$ only if $mR \gg 1$. In the constituent quark model to be described here, this is not satisfied for the u, d and s flavored quarks. We shall overlook this shortcoming here and note a point in the favor of the model — that the spurious excitation of the centre-of-mass motion can be eliminated easily in the nonrelativistic framework. This is vital for the correct counting and classification of the excited states. In the oscillator model described here, all this can be done analytically. The basis states are generated by the Hamiltonian

$$\mathcal{H}_0 = \frac{1}{2m}(\mathbf{p}_1^2 + \mathbf{p}_2^2) + \frac{1}{2m'}\mathbf{p}_3^2 + \frac{1}{2}K\sum_{i<j}(\mathbf{r}_i - \mathbf{r}_j)^2 \; . \tag{1.5.1}$$

Here quarks 1 and 2 are assumed to have the same mass, and quark 3 has mass m'. The mass difference between the u and d quarks are ignored. For N and Δ, $m = m'$; for Λ and Σ, $m' = m_s$. The quarks are confined in an oscillator potential whose slope is independent of the flavor quantum number. One defines the Jacobi coordinates to eliminate the $c.m.$ variables:

$$\boldsymbol{\rho} = \frac{(\mathbf{r}_1 - \mathbf{r}_2)}{\sqrt{2}} \; , \; \boldsymbol{\lambda} = \frac{(\mathbf{r}_1 + \mathbf{r}_2 - 2\mathbf{r}_3)}{\sqrt{6}} \; , \; \mathbf{R}_{cm} = \frac{m(\mathbf{r}_1 + \mathbf{r}_2) + m'\mathbf{r}_3}{(2m + m')} \; . \tag{1.5.2}$$

Note that the coordinate $\boldsymbol{\rho}$ is antisymmetric and $\boldsymbol{\lambda}$ symmetric under the exchange of $\mathbf{r}_1$ and $\mathbf{r}_2$, in conformity with our notation in spin and isospin wavefunctions. Define

$$M = 2m + m' \quad , \quad m_\rho = m \quad , \quad m_\lambda = \frac{3mm'}{(2m + m')} \quad , \tag{1.5.3}$$

and the momenta conjugate to $\boldsymbol{\rho}, \boldsymbol{\lambda}$ and $\mathbf{R}_{cm}$:

$$\mathbf{p}_\rho = m_\rho\dot{\boldsymbol{\rho}} \quad , \quad \mathbf{p}_\lambda = m_\lambda\dot{\boldsymbol{\lambda}} \quad , \quad \mathbf{P}_{cm} = M\dot{\mathbf{R}}_{cm} \; .$$

It is straightforward to check that the oscillator Hamiltonian reduces to

$$\mathcal{H}_0 = \left(\frac{p_\rho^2}{2m_\rho} + \frac{3}{2}K\rho^2\right) + \left(\frac{p_\lambda^2}{2m_\lambda} + \frac{3}{2}K\lambda^2\right) + \frac{P_{cm}^2}{2M} \; . \tag{1.5.4}$$

The last term corresponds to the *c.m.*, and does not play any role in the intrinsic spectrum of the baryon. Thus the intrinsic spatial degrees of freedom correspond to the motion of two independent oscillators in this model. The oscillator spacings

$$\omega_\rho = (3K/m_\rho)^{1/2} \quad , \quad \omega_\lambda = (3K/m_\lambda)^{1/2} \quad , \tag{1.5.5}$$

are identical in the N, Δ and Ω^- where $m = m'$. Henceforth we consider N and Δ, and put $\omega = \omega_\rho = \omega_\lambda = (3K/m)^{1/2}$. The spatial wave function is a product of the ρ-oscillator and the λ-oscillator states. Using standard notation, the principal quantum numbers of the ρ-oscillator is $N_\rho = (2n_\rho + \ell_\rho)$, and similarly for the λ-oscillator. The energy of a state is specified by the quantum number $\mathcal{N}$:

$$E_{\mathcal{N}} = (\mathcal{N} + \tfrac{3}{2})\omega \quad , \quad \mathcal{N} = N_\rho + N_\lambda = (2n_\rho + \ell_\rho) + (2n_\lambda + \ell_\lambda) \; .$$

The spatial angular momentum $\mathbf{L}$ of a state is obtained by coupling $\boldsymbol{\ell}_\rho$ and $\boldsymbol{\ell}_\lambda$:

$$\mathbf{L} = \boldsymbol{\ell}_\rho + \boldsymbol{\ell}_\lambda \; . \tag{1.5.6}$$

The wave function of an oscillator is (*e.g.* the ρ-oscillator)

$$\psi_{n_\rho \ell_\rho}(\boldsymbol{\rho}) = R_{n_\rho \ell_\rho}(\rho) Y_{\ell_\rho m_\ell}(\hat{\boldsymbol{\rho}}) \quad , \tag{1.5.7}$$

where we have dropped the m_ℓ-quantum number in $\psi_{n_\rho \ell_\rho}$ for simplicity. Denoting the total spatial wave function by $\Psi_{\mathcal{N}L}(\boldsymbol{\rho}, \boldsymbol{\lambda})$, the ground-state obviously has $\mathcal{N} = 0$, $L^\pi = 0^+$:

$$\Psi^S_{00}(\boldsymbol{\rho}, \boldsymbol{\lambda}) = \psi_{00}(\boldsymbol{\rho}) \psi_{00}(\boldsymbol{\lambda}) \; . \tag{1.5.8}$$

Taking normalized oscillator wave functions,

$$\Psi^S_{00}(\boldsymbol{\rho}, \boldsymbol{\lambda}) = \left(\frac{\alpha^{3/2}}{\pi^{3/4}} \right)^2 e^{-\alpha_0^2(\rho^2 + \lambda^2)/2} \; . \tag{1.5.9}$$

This is totally symmetric, as denoted by the superscript S since $(\rho^2 + \lambda^2) = \frac{1}{3}(\mathbf{r}_{12}^2 + \mathbf{r}_{23}^2 + \mathbf{r}_{31}^2)$. We have used the oscillator parameter α_0 in (1.5.9):

$$\alpha_0 = (m\omega)^{1/2} = (3Km)^{1/4} \; . \tag{1.5.10}$$

The $\mathcal{N} = 1$ states have $L^\pi = 1^-$, and have mixed symmetry (ρ- and λ-types):

$$\begin{aligned} \Psi^\rho_{11} &= \psi_{01}(\boldsymbol{\rho}) \psi_{00}(\boldsymbol{\lambda}) \quad , \\ \Psi^\lambda_{11} &= \psi_{00}(\boldsymbol{\rho}) \psi_{01}(\boldsymbol{\lambda}) \; . \end{aligned} \tag{1.5.11}$$

Table 1.4

$\Psi^S_{20} = \frac{1}{}$

$\Psi^\lambda_{20} = \frac{1}{\sqrt{2}}[$

$\Psi^\rho_{20} = -[\psi$

$\Psi^A_{21} = [\psi_{0}$

$\Psi^S_{22} = \frac{1}{\sqrt{2}}[$

$\Psi^\lambda_{22} = \frac{1}{\sqrt{2}}[$

$\Psi^\rho_{22} = [\psi_{0}$

Note that apart from
tional to $\rho Y_1^m(\hat{\rho})$, whic
the interchange of 1 a
frequently in use and n
appropriate symmetry
the spin-flavor wave fun
given in this section, it
ric states as required. T
denoted as $|\{SU_6\}B^{2S+}$
tiplet structure, B stan
angular momentum, an
states. The latter is den
Symmetric, Mixed
The wave func
$\mathbf{J} = \mathbf{L} + \mathbf{S}$. For exampl
$J = \frac{5}{2}, \frac{3}{2}$ and $\frac{1}{2}$. Since
metry (see Eq. 1.5.11),
$|\{70\}N, {}^4P_M\rangle$ and $|\{70\}$
and $3/2^-, 1/2^-$) as shown
$\mathcal{N} = 1$ only $|\{70\}\Delta, {}^2P_M$
and $\Delta(1700)3/2^-$ states
The experimental d
Amongst the $\mathcal{N} = 2$ eve
configurations are seen
hand, with the exceptio
tain, or not seen at all. T

nd does not play any role in
the intrinsic spatial degrees of
n(ndent oscillators in this

$(3K/m_\lambda)^{1/2}$, (1.5.5)

$= m'$. Henceforth we consider
$)^{1/2}$. The spatial wave function
cillator states. Using standard
the ρ-oscillator is $N_\rho = (2n_\rho +$
energy of a state is specified

$(2n_\rho + \ell_\rho) + (2n_\lambda + \ell_\lambda)$.

te is obtained by coupling $\boldsymbol{\ell}_\rho$

(1.5.6)

he ρ-oscillator)

$_{,m_\ell}(\hat{\rho})$, (1.5.7)

umber in $\psi_{n_\rho \ell_\rho}$ for simplicity.
v $\Psi_{\mathcal{N}L}(\boldsymbol{\rho}, \boldsymbol{\lambda})$, the ground-state

$_{00}$. (1.5.8)

s.

$^2_0(\rho^2+\lambda^2)/2$. (1.5.9)

superscript S since $(\rho^2+\lambda^2) =$
ıtor parameter α_0 in (1.5.9):

$m)^{1/4}$. (1.5.10)

ave mixed symmetry (ρ- and

$\lambda)$,
(1.5.11)
$\lambda)$.

Table 1.4 $\mathcal{N} = 2$ Oscillator states

$$\Psi^S_{20} = -\frac{1}{\sqrt{2}}\left[\psi_{00}(\boldsymbol{\rho})\psi_{10}(\boldsymbol{\lambda}) + \psi_{10}(\boldsymbol{\rho})\psi_{00}(\boldsymbol{\lambda})\right]$$
$$\Psi^\lambda_{20} = \frac{1}{\sqrt{2}}\left[\psi_{00}(\boldsymbol{\rho})\psi_{10}(\boldsymbol{\lambda}) - \psi_{10}(\boldsymbol{\rho})\psi_{00}(\boldsymbol{\lambda})\right]$$
$$\Psi^\rho_{20} = -\left[\psi_{01}(\boldsymbol{\rho})\psi_{01}(\boldsymbol{\lambda})\right]^{L=0}$$
$$\Psi^A_{21} = \left[\psi_{01}(\boldsymbol{\rho})\psi_{01}(\boldsymbol{\lambda})\right]^{L=1}$$
$$\Psi^S_{22} = \frac{1}{\sqrt{2}}\left[\psi_{02}(\boldsymbol{\rho})\psi_{00}(\boldsymbol{\lambda}) + \psi_{00}(\boldsymbol{\rho})\psi_{02}(\boldsymbol{\lambda})\right]$$
$$\Psi^\lambda_{22} = \frac{1}{\sqrt{2}}\left[\psi_{02}(\boldsymbol{\rho})\psi_{00}(\boldsymbol{\lambda}) - \psi_{00}(\boldsymbol{\rho})\psi_{02}(\boldsymbol{\lambda})\right]$$
$$\Psi^\rho_{22} = \left[\psi_{01}(\boldsymbol{\rho})\psi_{01}(\boldsymbol{\lambda})\right]^{L=2}$$

S'

Note that apart from a spherically symmetric factor, $\psi_{01}(\rho)$ is proportional to $\rho Y_1^m(\hat{\rho})$, which transforms as $\boldsymbol{\rho}$, and hence changes sign under the interchange of 1 and 2. We also list the $\mathcal{N} = 2$ states which are frequently in use and may have $L^\pi = 0^+, 1^+$ or 2^+. Oscillator states of appropriate symmetry for $\mathcal{N} = 3$ will be found in ref. 47 . Combining the spin-flavor wave functions listed in Table 1.3 with the oscillator states given in this section, it is straightforward to construct totally symmetric states as required. These are listed for N and Δ below, with a state denoted as $|\{SU_6\}B^{2S+1}L_{\rm sym}\rangle$. Here, $\{SU_6\}$ denotes the spin-flavor multiplet structure, B stands for the baryon, spin $S = \frac{1}{2}$ or $\frac{3}{2}$, L the orbital angular momentum, and (sym) denotes the symmetry of the oscillator states. The latter is denoted by the subscript S, M or A corresponding to Symmetric, Mixed or Antisymmetric oscillator state.

The wave functions shown in Table 1.5 are still to be coupled to $\mathbf{J} = \mathbf{L} + \mathbf{S}$. For example, $|\{70\}N, {}^4P_M\rangle$ would couple to yield the states $J = \frac{5}{2}, \frac{3}{2}$ and $\frac{1}{2}$. Since the $\mathcal{N} = 1, L = 1^-$ states are of mixed symmetry (see Eq. 1.5.11), the low-lying odd-parity states of the nucleon are $|\{70\}N, {}^4P_M\rangle$ and $|\{70\}N, {}^2P_M\rangle$, giving rise to the five states ($5/2^-$, $3/2^-$, $1/2^-$ and $3/2^-$, $1/2^-$) as shown in Table 1.1 . For the Δ, on the other hand, for $\mathcal{N} = 1$ only $|\{70\}\Delta, {}^2P_M\rangle$ is allowed by symmetry, yielding the $\Delta(1620)1/2^-$ and $\Delta(1700)3/2^-$ states in Table 1.1 .

The experimental data in the table show a very interesting pattern. Amongst the $\mathcal{N} = 2$ even-parity excited states, only the symmetric $\{56\}$ configurations are seen strongly. The $\{70\}$ $\mathcal{N} = 2$ states, on the other hand, with the exception of $N(1710)1/2^+$, are either very weak and uncertain, or not seen at all. This, of course, in not the case with the $\mathcal{N} = 1$ $\{70\}$

Table 1.5 Symmetrised States of N and Δ

Nucleon

$$|\{56\}N,{}^2L_S\rangle = \tfrac{1}{\sqrt{2}}(\chi^\rho\phi^\rho + \chi^\lambda\phi^\lambda)\Psi^S_{\mathcal{N}L} \quad ,$$

$$|\{70\}N,{}^2L_M\rangle = \tfrac{1}{2}[(\chi^\rho\phi^\lambda + \chi^\lambda\phi^\rho)\Psi^\rho_{\mathcal{N}L} + (\chi^\rho\phi^\rho - \chi^\lambda\phi^\lambda)\Psi^\lambda_{\mathcal{N}L}] \quad ,$$

$$|\{70\}N,{}^4L_M\rangle = \tfrac{1}{\sqrt{2}}(\phi^\rho\Psi^\rho_{\mathcal{N}L} + \phi^\lambda\Psi^\lambda_{\mathcal{N}L})\chi^S \quad ,$$

$$|\{20\}N,{}^2L_A\rangle = \tfrac{1}{\sqrt{2}}(\chi^\rho\phi^\lambda - \chi^\lambda\phi^\rho)\Psi^A_{\mathcal{N}L} \quad ,$$

Delta

$$|\{56\}\Delta,{}^4L_S\rangle = \chi^S\phi^S\Psi^S_{\mathcal{N}L} \quad ,$$

$$|\{70\}\Delta,{}^2L_M\rangle = \tfrac{1}{\sqrt{2}}(\chi^\rho\Psi^\rho_{\mathcal{N}L} + \chi^\lambda\Psi^\lambda_{\mathcal{N}L})\phi^S \ .$$

odd-parity states, all of which are seen. Table 1.4 shows that a state like Ψ^ρ_{2L} has both the ρ- and λ-coordinates excited together, and these constitute half the weight of the $\{70\}$ $\mathcal{N}=2$ wave functions (Table 1.5). Such states do not couple directly to the ground state through a single-quark excitation process. This is easiest to see with $\mathbf{r}_3 = \mathbf{R} - \sqrt{2/3}\,\boldsymbol{\lambda}$. A one-body operator coupling to quark 3 may only cause excitation of the λ-oscillator. Since the total wave function is overall symmetric the matrix element of an operator O_i $(i = 1,2,3)$ is

$$\langle O_i\rangle = 3\langle O_3\rangle \ . \tag{1.5.12}$$

It follows that Ψ^ρ_{2L} and Ψ^A_{21} states would be hard to excite through one-step processes.

Note that the elimination of the *c.m.* coordinate $\mathbf{R}$ is crucial in the correct counting of the states. This is one reason why the nonrelativistic approach is so successful in spectroscopy. To gain further insight, the oscillator basis may be used to diagonalize the interaction between the quarks. If one ignores the spin-orbit part of the one-gluon exchange potential, then the spin-dependent piece between two quarks i and j in a baryon is[45]

$$V^{ij}_{hf} = \frac{2\alpha_s}{3m_im_j}\left[\frac{8\pi}{3}\mathbf{S}_i\cdot\mathbf{S}_j\delta^3(\mathbf{r}_{ij}) + \frac{1}{r^3_{ij}}\left(\frac{3(\mathbf{S}_i\cdot\mathbf{r}_{ij})(\mathbf{S}_j\cdot\mathbf{r}_{ij})}{r^2_{ij}} - \mathbf{S}_i\cdot\mathbf{S}_j\right)\right] \ . \tag{1.5.13}$$

The spin-independent Coulomb potential and other momentum-dependent terms have been left out. The effective quark-gluon coupling constant α_s (analogous to the electromagnetic coupling constant $\alpha = 1/137$) is determined by calculating the N-Δ mass difference with V_{hf} of Eq. (1.5.13) in

V and Δ

$'L$

$_{VL} + (\chi^\rho\phi^\rho - \chi^\lambda\phi^\lambda)\Psi^\lambda_{NL}]$,

$_{L})\chi^S$,

$_{VL}$,

$_{L})\phi^S$.

seen. Table 1.4 shows that a state
dinates excited together, and these
$\mathcal{N} = 2$ wave functions (Table 1.5).
the ground state through a single-
iest to see with $\mathbf{r}_3 = \mathbf{R} - \sqrt{2/3}\,\boldsymbol{\lambda}$. A
3 may only cause excitation of the
tion is overall symmetric the matrix
) is

$$3\langle O_3\rangle \ . \qquad (1.5.12)$$

ould be hard to excite through one-

c.m. coordinate $\mathbf{R}$ is crucial in the
i e reason why the nonrelativis-
roscopy. To gain further insight, the
gonalize the interaction between the
part of the one-gluon exchange po-
ce between two quarks i and j in a

$$\frac{1}{\,_{ij}}\left(\frac{3(\mathbf{S}_i\cdot\mathbf{r}_{ij})(\mathbf{S}_j\cdot\mathbf{r}_{ij})}{r_{ij}^2} - \mathbf{S}_i\cdot\mathbf{S}_j\right)\Bigg] \ . \qquad (1.5.13)$$

ntial and other momentum-dependent
ive quark-gluon coupling constant α_s
oupling constant $\alpha = 1/137$) is deter-
difference with V_{hf} of Eq. (1.5.13) in

this model. It is important to realize that this value of α_s depends on how large an oscillator basis is chosen for the diagonalization of V_{hf}. A very large basis would cause a collapse of N due to the zero-range attractive interaction, so α_s would be infinitesimal. On the other hand, the simplest approximation is to take the pure $\mathcal{N} = 0$ oscillator states:

$$|N\rangle = |\{56\}N, {}^2S_S\rangle \quad , \quad |\Delta\rangle = |\{56\}\Delta, {}^4S_S\rangle \quad , \qquad (1.5.14)$$

giving α_s close to unity.

Exercise 1.7

Using the form (1.5.14), show that in first-order perturbation theory,

$$M_\Delta - M_N = 2\sqrt{2}\,\alpha_s\alpha_0^3/3m^2\sqrt{\pi} \ .$$

The oscillator state Ψ^S_{00} is defined in Eq. (1.5.9), with $\alpha_0 = (m\omega)^{1/2}$. Taking $\omega = 0.5\,\mathrm{GeV}$, $m = 0.33\,\mathrm{GeV}$, show that $\alpha_s = 0.9$ to fit the experimental mass splitting between Δ and N. Use the property (1.5.12) to evaluate $\langle V^{12}_{hf}\rangle$, and multiply it by three.

Isgur and Karl[46] originally took an oscillator space up to $\mathcal{N} = 2$ to do most of the calculations. Recently, a larger basis has been used for diagonalization[47]. The hyperfine interaction would cause the simple wave functions (1.5.14) to be modified, causing the nucleon and delta ground states to have small admixtures of excited basis states. For a basis up to $\mathcal{N} = 2$, they find, for example[48],

$$|N\rangle \approx 0.90|\{56\}N, {}^2S_S\rangle - 0.34|\{56\}N, {}^2S'_S\rangle - 0.27|\{70\}N, {}^2S_M\rangle - 0.06|\{70\}N, {}^2D_M\rangle \ . \qquad (1.5.15)$$

The D-state mixing is caused by the tensor interaction in V^{ij}_{hf}, as given by the second term in the right-hand side of (1.5.13), which acts only in the $S = 1$ state of a pair. The $\mathbf{S}_1\cdot\mathbf{S}_2$ term also is repulsive for the $S = 1$ state, and attractive for $S = 0$. For the pair uu in proton and dd in neutron, $S = 1$, and this causes a repulsion between like quarks. This is why the nucleon (or Δ) wave functions are no longer totally spatially symmetric.

Exercise 1.8

Calculate the mean square charge radius

$$\langle r^2\rangle_{\text{ch}} = \sum_{i=1}^{3} \langle e_i(\mathbf{r}_i - \mathbf{R})^2\rangle \quad ,$$

for the neutron and the proton ground states, taking the pure oscillator states (1.5.14). It will be easy if you take $\langle r^2\rangle_{\text{ch}} = 3\langle e_3(\mathbf{r}_3 - \mathbf{R})^2\rangle$, and note that $(\mathbf{r}_3 - \mathbf{R})^2 = \frac{2}{3}\lambda^2$. Recall that (in units of charge e)

$$e_3 = \left(\tfrac{1}{2}Y(3) + I_3(3)\right) \quad ,$$

where $Y = (B + S)$ is the hypercharge, and $I_3 = \tau_3/2$. You should find

$$\langle e_3\rangle_P = \frac{1}{3} \quad , \quad \langle e_3\rangle_n = 0 \quad .$$

and

$$\langle r^2\rangle^P_{\text{ch}} = \alpha_0^{-2} \quad \text{for proton} \quad , \quad \langle r^2\rangle^n_{\text{ch}} = 0 \quad \text{for neutron} \quad .$$

The above exercise shows that for a purely symmetric state given by (1.5.14), the neutron charge radius is zero. The experimental value of $\langle r^2\rangle^n_{\text{ch}}$ is small and negative as given by Eq. (1.2.8). Taking the state (1.5.15) for $|N\rangle$ that has admixtures of $|\{70\}, {}^2S_M\rangle$ wave function, it was shown that one obtains a realistic value for the ratio $\langle r^2\rangle^n_{\text{ch}}/\langle r^2\rangle^P_{\text{ch}}$. Note, however, that the charge radius $\langle r^2\rangle^P_{\text{ch}}$ is 0.49 fm only if the oscillator spacing ω is taken to be 500 MeV to fit the odd-parity excited states. This is far too small compared to the experimental value given in Eq. (1.2.8).

Exercise 1.9

Consider each quark as a point Dirac particle. In the nonrelativistic limit, the magnetic moment operator is

$$\boldsymbol{\mu} = \sum_{i=1}^{3} \frac{e_i e}{2m_i}\boldsymbol{\sigma}_i \quad , \quad \mathbf{s}_i = \tfrac{1}{2}\boldsymbol{\sigma}_i \ .$$

(a) Calculate $\langle N|\mu_z|N\rangle$ fo
Show that

$$\mu_P = \frac{}{2}$$

and $\mu_n = -$

(b) Show that the transiti

$$\mu_{\Delta P}$$

where again only the {

From the calculation o
we see that the experimer
close to the theoretical val
step further, the calculatio
may be reproduced by tal
mass. This gives the "cons
third the nucleon mass. It i
350 MeV. This is very diff
enter the Lagrangian in a
current quark masses of u
on the bag model, we shal
zero-mass quark is not to
more sophisticated ap
dynamical chiral symmetry
It may be worthwhile l
helicity amplitudes $A_{3/2}$ ar
and comment on the role of
interaction in the nonrelati

$$H^{\text{em}}_{\text{int}} = \sum_{i=1}^{3} -\frac{e_i e}{2m_i}\left[(\mathbf{p}_i \cdot \mathbf{A}(\right.$$

If one takes, for the odd-
1 state, and for the grou
wave function, some simple
follow. For example, consid

$N(167$

dı..

$- \mathbf{R})^2\rangle$,

states, taking the pure oscillator
ake $\langle r^2\rangle_{\rm ch} = 3\langle e_3(\mathbf{r}_3 - \mathbf{R})^2\rangle$, and
(in units of charge e)

$I_3(3))$,

and $I_3 = \tau_3/2$. You should find

$\langle r^2\rangle^n_{\rm ch} = 0$ for neutron .

ır a purely symmetric state given
ıs is zero. The experimental value
en by Eq. (1.2.8). Taking the state
of $|\{70\}, {}^2S_M\rangle$ wave function, it was
u · the ratio $\langle r^2\rangle^n_{\rm ch}/\langle r^2\rangle^P_{\rm ch}$. Note,
$)^P_{\rm ch}$ is 0.49 fm only if the oscillator
t the odd-parity excited states. This
rimental value given in Eq. (1.2.8).

Dirac particle. In the nonrelativistic
r is

, $\mathbf{s}_i = \frac{1}{2}\boldsymbol{\sigma}_i$.

(a) Calculate $\langle N|\mu_z|N\rangle$ for n and P, using the wave functions (1.5.14). Show that

$$\mu_P = \frac{e}{2m} \quad , \quad \text{where we take} \quad m_u = m_d = m$$

and

$$\mu_n = -\frac{2}{3}\frac{e}{2m} \ .$$

(b) Show that the transition magnetic moment is

$$\mu_{\Delta P} = \langle \Delta^+|\mu_z|P\rangle = \frac{2\sqrt{2}}{3}\mu_P \quad ,$$

where again only the $\{56\}$ symmetric ground state is taken.

From the calculation of the magnetic moments in the above exercise, we see that the experimental ratio of $\mu_n/\mu_P \approx -1.91/2.79 = -0.68$ is close to the theoretical value of $-\frac{2}{3}$, irrespective of the mass m. Going a step further, the calculation also shows that the proton magnetic moment may be reproduced by taking $m = M_P/2.79$, where M_P is the proton mass. This gives the "constituent" quark mass $m \approx 336$ MeV, about one third the nucleon mass. It is customary to choose m within the range 300–350 MeV. This is very different from the "current" quark masses which enter the Lagrangian in a relativistic formulation (see Section 5.5). The current quark masses of u and d quarks are only a few MeV. In Chapter 4 on the bag model, we shall see that the zero-point energy of a confined zero-mass quark is not too different from the constituent mass[49]. In a more sophisticated approach, the constituent quark mass is generated by dynamical chiral symmetry breaking (see Ex. 4.8).

It may be worthwhile here to go back briefly to the photoproduction helicity amplitudes $A_{3/2}$ and $A_{1/2}$ that were introduced in Section (1.3), and comment on the role of the hyperfine interaction. The electromagnetic interaction in the nonrelativistic form (neglecting the A^2 term) is[50]

$$H^{\rm em}_{\rm int} = \sum_{i=1}^{3} -\frac{e_i e}{2m_i}\left[(\mathbf{p}_i \cdot \mathbf{A}(r_i) + \mathbf{A}(\mathbf{r}_i)\cdot \mathbf{p}_i) + \boldsymbol{\sigma}_i \cdot (\boldsymbol{\nabla}_i \times \mathbf{A}(\mathbf{r}_i))\right] \ . \quad (1.5.16)$$

If one takes, for the odd-parity $\mathcal{N} = 1$ excited state a pure $\{70\}$ $L = 1$ state, and for the ground state of the nucleon a pure $\{56\}$ $L = 0$ wave function, some simple selection rules, first observed by Moorhouse[51], follow. For example, consider the electromagnetic decays of

$$N(1675)5/2^- \to N(940)1/2^+ + \gamma \ .$$

Again take $H_{\rm int}^{\rm em} = 3H_{\rm int}^{\rm em}(3)$, exploiting the overall symmetry. From Table 1.5, $N(1675)^5\!/\!_2{}^-$ belongs to $|\{70\}N, {}^4P\rangle$ state, with a symmetric spin function χ^S. An operator $H_{\rm int}(3)$, depending only on the coordinates of quark 3, cannot alter the wave function of 1 and 2. Since χ^ρ and χ^S are orthogonal in this part, only the λ-part contributes:

$$\langle\{70\}N, {}^4P_M|e_3|\{56\}N, {}^2S_S\rangle = \tfrac{1}{2}\langle\phi^\lambda|e_3|\phi^\lambda\rangle \; .$$

It is easy to check that for the proton, $\langle\phi^\lambda_{1/2}|e_3|\phi^\lambda_{1/2}\rangle = 0$ while for the neutron $\langle\phi^\lambda_{-1/2}|e_3|\phi^\lambda_{-1/2}\rangle = \frac{1}{3}$. It then follows that the $N(1675)^5\!/\!_2{}^- \to p\gamma$ $A^P_{3/2}$ and $A^P_{1/2}$ amplitudes should vanish, while the corresponding $n\gamma$ transitions may be appreciable. Experimentally[26],

$$\begin{aligned} A^n_{3/2} &= -69 \pm 19 \quad , \quad A^n_{1/2} = -47 \pm 23 \quad , \\ A^P_{3/2} &= 19 \pm 12 \quad , \quad A^P_{1/2} = 19 \pm 12 \quad , \end{aligned}$$

in units of $\mathrm{GeV}^{-1/2} \times 10^{-3}$. The deviations from the ideal Moorhouse predictions are due to the spin-dependent forces that have caused the admixtures of the $\{70\}$ states in the ground state. Similar predictions in the strange sector $\Lambda(1830)^5\!/\!_2{}^- \to \bar{K}N$ are also modified by such mixings[48]. These examples show the usefulness of the Isgur-Karl model. Taking such diagonalized wave functions, Isgur and Koniuk[30] also analyzed which excited states would couple strongly in the pion channel. This provided an explanation to the puzzle of the "missing resonances".

We briefly refer to another curious aspect of the spectrum in Table 1.1 — that the even parity excitations are at about the same energy as the odd-parity ones. Indeed, $N(1440)^1\!/\!_2{}^+, \Lambda(1600)^1\!/\!_2{}^+$ and $\Sigma(1660)^1\!/\!_2{}^+$ excitations all seem to be anomalously low in the oscillator model. In the standard Isgur-Karl picture, this is attributed to the anharmonic forces present in the qq-interaction, that tend to bring down the symmetric states much more than the mixed symmetric ones. What are the anharmonic interactions? The point to note is that the harmonic form $\mathcal{H}_0$ of Eq. (1.5.1) was assumed for convenience. A more realistic spin-independent form of the Hamiltonian, dictated by theory and meson spectroscopy, would be

$$\mathcal{H}_0' = \frac{1}{2m}(\mathbf{p}_1^2 + \mathbf{p}_2^2) + \frac{1}{2m'}p_3^2 + \sum_{i<j}\left(-\frac{2}{3}\frac{\alpha_s}{r_{ij}} + \frac{1}{2}br_{ij}\right) \; . \tag{1.5.17}$$

Here b is the universal confinement strength of about $0.18\,\mathrm{GeV}^2$ obtained from the spectroscopy of heavy mesons, and α_s the effective quark-gluon

coupling. The origin c
tial is due to th
independent part of th
harmonic form assume
the ground state, but t
ciably. An essentially e
however, that $N(1440$
harmonicity. Similar pr
and $\Delta(1930)^5\!/\!_2{}^-$ states
which assumed that in
body forces in the bary
the excited states. It is
states without introduc

Exercise 1.10 Th

In N and Δ, assu
triaxial oscillator, with

$$\mathcal{H}_0 = \frac{1}{2m}$$

Show that the intrinsic

$$E_{N_xN_yN_z} = \hbar\omega_x($$

where

$$N_x = (n_{\rho_x} + n_{\lambda_x}) \; .$$

To determine the defor $E_{N_xN_yN_z}$ by varying ω_x,

Show that this leads to

$$\omega_x(N_x +$$

Define $\mathcal{N} = N_x + N_y +$ $\omega_x = \omega_y = \omega_z = \omega_0$ fro as the standard Isgur-Ka state is prolate, with E_0

overall symmetry. From Ta-
) state, with a symmetric spin
ly on the coordinates of
1 and 2. Since χ^ρ and χ^S are
itributes:

$$= \frac{1}{2}\langle\phi^\lambda|e_3|\phi^\lambda\rangle \ .$$

$\phi^\lambda_{1/2}|e_3|\phi^\lambda_{1/2}\rangle = 0$ while for the
ows that the $N(1675)^5/_2^- \rightarrow$
1, while the corresponding $n\gamma$
itally[26],

$$= -47 \pm 23 \quad ,$$

$$= 19 \pm 12 \quad ,$$

ons from the ideal Moorhouse
forces that have caused the ad-
state. Similar predictions in the
so modified by such mixings[48].
Isgur-Karl model. Taking such
oniuk[30] also analyzed which ex-
pion channel. This provided an
resonances".
ect of the spectrum in Table 1.1
it the same energy as the
$16..)^1/_2^+$ and $\Sigma(1660)^1/_2^+$ exci-
in the oscillator model. In the
buted to the anharmonic forces
bring down the symmetric states
es. What are the anharmonic in-
harmonic form $\mathcal{H}_0$ of Eq. (1.5.1)
alistic spin-independent form of
meson spectroscopy, would be

$$\left(-\frac{2}{3}\frac{\alpha_s}{r_{ij}} + \frac{1}{2}br_{ij}\right) \ . \qquad (1.5.17)$$

gth of about 0.18 GeV^2 obtained
and α_s the effective quark-gluon

coupling. The origin of the numerical factor $-\frac{2}{3}$ in the Coulomb potential is due to the color factor $\langle\boldsymbol{\lambda}_i/2 \cdot \boldsymbol{\lambda}_j/2\rangle$, see Eq. (3.3.22). The spin-independent part of the interaction is thus appreciably different from the harmonic form assumed to generate the basis. This should not matter for the ground state, but the higher excited state positions would alter appreciably. An essentially exact three-body calculation[52] with (1.5.17) shows, however, that $N(1440)^1/_2^+$ cannot have come down so low due to anharmonicity. Similar problems are encountered in the $\mathcal{N} = 3$ $\Delta(1900)^1/_2^-$ and $\Delta(1930)^5/_2^-$ states. There have been variations of the oscillator model which assumed that in addition to $\mathcal{H}_0'$ of Eq. (1.5.17), there are many-body forces in the baryon that may cause deformation[53] of the baryon in the excited states. It is then possible to bring down the $\mathcal{N} = 2$ and $\mathcal{N} = 3$ states without introducing extra parameters.

Exercise 1.10 The Deformed Oscillator Model[53]

In N and Δ, assume that the quarks are moving in a deformable triaxial oscillator, with

$$\mathcal{H}_0 = \frac{1}{2m}(p_\rho^2 + p_\lambda^2) + \frac{1}{2}m \sum_{j=x,y,z} \omega_j^2(\rho_j^2 + \lambda_j^2) \ .$$

Show that the intrinsic energy may be written as

$$E_{N_xN_yN_z} = \hbar\omega_x(N_x + 1) + \hbar\omega_y(N_y + 1) + \hbar\omega_z(N_z + 1) \quad ,$$

where

$$N_x = (n_{\rho_x} + n_{\lambda_x}) \quad , \quad N_y = (n_{\rho_y} + n_{\lambda_y}) \quad , \quad N_z = (n_{\rho_z} + n_{\lambda_z}) \ .$$

To determine the deformation for a given set (N_x, N_y, N_z), minimize $E_{N_xN_yN_z}$ by varying ω_x, ω_y and ω_z, with the constant volume condition

$$\omega_x\omega_y\omega_z = \omega_0^3 \ .$$

Show that this leads to

$$\omega_x(N_x + 1) = \omega_y(N_y + 1) = \omega_z(N_z + 1) \ .$$

Define $\mathcal{N} = N_x + N_y + N_z$. Note that for $\mathcal{N} = 0$, the ground-state, $\omega_x = \omega_y = \omega_z = \omega_0$ from above, so the baryon is spherical, the same as the standard Isgur-Karl model. Show that for $\mathcal{N} = 1$, the equilibrium state is prolate, with $E_{001} = 3.78\,\omega_0$ (instead of $(3/2 + 5/2)\omega_0 = 4\omega_0$ of the spherical model). Also show that the lowest $\mathcal{N} = 2$ state is prolate, with energy $E_{002} = 4.32\omega_0$. The energy difference between the $\mathcal{N} = 3$ and $\mathcal{N} = 2$ states is now $(4.32 - 3.78)\omega_0 = 0.54\omega_0$, rather than ω_0 of the spherical model. Further lowering will result from projecting out the $L = 0$ state.

From Table 1.1, we see that there are very small spin-orbit splittings in the data. For example, $N(1520)3/2^-$ and $N(1535)1/2^-$ are really degenerate, as are the $\mathcal{N} = 2$ $^4 10$ states in Δ around 1910–1950 MeV. If one took the two-body spin-orbit part of the one-gluon exchange potential, and eliminated the *c.m.* coordinate, one gets the form[54]

$$V_{SO}^{G} = \frac{3\alpha_s}{4\sqrt{2}\,m^2}\frac{1}{\rho^3}\left\{(\boldsymbol{\sigma}_1 + \boldsymbol{\sigma}_2)\cdot(\boldsymbol{\rho}\times \mathbf{p}_\rho) - \frac{1}{3\sqrt{3}}(\boldsymbol{\sigma}_1 - \boldsymbol{\sigma}_2)\cdot(\boldsymbol{\rho}\times \mathbf{p}_\lambda)\right\} \quad , \tag{1.5.18}$$

where we have multiplied by 3 to take account of three pairs in N or Δ. A direct diagonalization of this would totally destroy agreement of the model with experiment. Note, however, that the spin-orbit potential V_{SO}^{G} is of long range, in contrast to the "zero-range" $\boldsymbol{\sigma}_1 \cdot \boldsymbol{\sigma}_2$ potential. The strength α_s in the latter was dependent on the size of the basis, and this was due to its extreme short range character. If one knew what the actual range of the $\boldsymbol{\sigma}_1 \cdot \boldsymbol{\sigma}_2$ force is, one could do a nonperturbative[54] (or a large basis[47]) calculation to fix α_s, and use this in Eq. (1.5.18). Calculation along these lines indicate a much smaller[47] α_s, and moreover there are other effects (like cancellation[46] with the one-body spin-orbit potential arising through relativistic effects) that result in the suppresion of the spin-orbit force[55]. Actually, contrary to the claims in the literature, there is still considerable ambiguity in the model. There are several sophisticated versions of the oscillator model in the literature, but the most useful is still the simplest Isgur-Karl version originally proposed.

References

1. Abraham Pais, "Inward Bound" (Clarendon Press, Oxford, 1968), p. 189.
2. H. Geiger and E. Marsden, *Proc. Roy. Soc.* **A82**, 495 (1909).
3. M. Breidenbach *et al.*, *Phys. Rev. Lett.* **23**, 935 (1969).]
4. J. D. Bjorken, *Phys. Rev.* **179**, 1547 (1969);
   R. P. Feynman, *Phys. Rev. Lett.* **23**, 1415 (1969); *Science*. **183**, 601 (1974).

5. T. Eichten *et al.*
6. A. Benventu
7. D. H. Perkin
   1980 (Ed. J. H.
   also his paper in
8. E. Fermi, *Nuovo*
9. F. Halzen and A
   New York, 1984)
10. F. E. Close, "Qu
11. See, for example
    the Nucleus" (A
12. J. L. Friar, in Ne
    B: Physics Vol. 1
    Press, New York
13. R. G. Arnold *et*
    D. W. L. Sprung
14. G. G. Simon *et*
15. L. Koester *et al.*,
16. G. G. Simon *et*
17. S. R. Amendolia
    B277, 168 (1986
18. K. L. Miller *et a*
19. W. B. Atwood,
    Chromodynamic
    and D. Ruell B
20. J. J. Aubert
    To appear in *Nu*
21. C. G. Callan and
22. J. J. Aubert *et a*
23. A. Bodek *et al.*,
24. R. G. Arnold *et*
    3257.
25. G. B. West, *Phy*
26. Revs. of Particle
27. See, for example,
    Wesley, Reading.
28. R. E. Cutkosky *e*
    ibid 2839 (1979).

the lowest $\mathcal{N} = 2$ state is prolate,
rgy difference between the $\mathcal{N} = 3$
8 $= 0.54\,\omega_0$, rather than ω_0 of
w... result from projecting out the

---

are very small spin-orbit splittings
and $N(1535)\frac{1}{2}^-$ are really degen-
Δ around 1910–1950 MeV. If one
the one-gluon exchange potential,
ne gets the form[54]

$$
\rho) - \frac{1}{3\sqrt{3}}(\boldsymbol{\sigma}_1 - \boldsymbol{\sigma}_2) \cdot (\boldsymbol{\rho} \times \mathbf{p}_\lambda) \Big\} \quad , \tag{1.5.18}
$$

account of three pairs in N or Δ. A
tally destroy agreement of the model
t the spin-orbit potential V^G_{SO} is of
nge" $\boldsymbol{\sigma}_1 \cdot \boldsymbol{\sigma}_2$ potential. The strength
e size of the basis, and this was due
If one knew what the actual range of
nperturbative[54] (or a large basis[47])
Eq. (1.5.18). Calculation along these
nd moreover there are other effects
spin-orbit potential arising through
suppresion of the spin-orbit force[55].
ature, there is still considerable
several sophisticated versions of the
the most useful is still the simplest
d.

" (Clarendon Press, Oxford. 1968),

c. *Roy. Soc.* **A82**, 495 (1909).
v. *Lett.* **23**, 935 (1969).]
1547 (1969);
. **23**, 1415 (1969); *Science.* **183**, 601

5. T. Eichten *et al.*, *Phys. Lett.* **B46**, 274 (1973).
6. A. Benventuti *et al.*, *Phys. Rev. Lett.* **32**, 800 (1974).
7. D. H. Perkins, in "The Nature of Matter", Wolfson College Lectures 1980 (Ed. J. H. Mulvey, Clarendon Press, Oxford, 1981) p. 81. See also his paper in *Contemp. Phys.* **16**, 173 (1975).
8. E. Fermi, *Nuovo Cim.* **11**, 1 (1934).
9. F. Halzen and A. D. Martin, "Quarks and Leptons", (John Wiley, New York, 1984).
10. F. E. Close, "Quarks and Partons", (Academic Press, London, 1979).
11. See, for example, M. A. Preston and R. K. Bhaduri, "Structure of the Nucleus" (Addison-Wesley, Reading, MA, 1975).
12. J. L. Friar, in New Vistas in Electro-Nuclear Physics, Nata ASI Series B: Physics Vol. **142**, 213 (1986). (Eds. E. L. Tomusiak *et al.*, Plenum Press, New York).
13. R. G. Arnold *et al.*, *Phys. Rev. Lett.* **35**, 776 (1975),
    D. W. L. Sprung and K. Srinivasa Rao, *Phys. Lett.* **53B**, 397 (1975)
14. G. G. Simon *et al.*, *Nucl. Phys.* **A333**, 381 (1980).
15. L. Koester *et al.*, *Phys. Rev. Lett.* **36**, 1021 (1976).
16. G. G. Simon *et al.*. *Z. Naturforsch.* **35A**, 1 (1980).
17. S. R. Amendolia *et al.*, *Phys. Lett.* **138B**, 545 (1984); *Nucl. Phys.* **B277**, 168 (1986).
18. K. L. Miller *et al.*, *Phys. Rev.* **D26**, 537 (1982).
19. W. B. Atwood, in "Lectures on Lepton Scattering and Quantum Chromodynamics", Progress in Physics, Vol. 4 (Edited by A. Jaffe and D. Ruelle, Birkäuser, Boston, 1982).
20. J. J. Aubert *et al.*, (EMC collaboration), CERN EP/86-66 (1987) To appear in *Nucl. Phys. B.*
21. C. G. Callan and D. Gross, *Phys. Rev. Lett.* **22**, 156 (1969).
22. J. J. Aubert *et al.*, *Phys. Lett.* **123B**, 275 (1983).
23. A. Bodek *et al.*, *Phys. Rev. Lett.* **50**, 1431 (1983), **51**, 534 (1983).
24. R. G. Arnold *et al.*, *Phys. Rev. Lett.* **52**, 727 (1984); SLAC-PUB-3257.
25. G. B. West, *Phys. Rep.* **18**, 264 (1975).
26. Revs. of Particle Properties, *Phys. Lett.* **170B**, 1 (1986).
27. See, for example, G. Kallen, "Elementary Particle Physics" (Addison-Wesley, Reading, MA, 1964).
28. R. E. Cutkosky *et al.*, *Phys. Rev.* **D20**, 2782 (1979); ibid 2804 (1979); ibid 2839 (1979).

29. R. Koch and E. Pietarinen, *Nucl. Phys.* **A336**, 331 (1980;)
G. Höhler, Proc. Third LAMPF II Workshop, Vol. 1, 334, (1983).

30. R. Koniuk and N. Isgur, *Phys. Rev.* **D21**, 1868 (1980);
R. Koniuk, *Nucl. Phys.* **B195**, 452 (1982);
N. Isgur, Proc. 1984 CEBAF Summer Workshop, 199 (1984) (eds. F. Gross and R. Whitney, CEBAF report, Newport News, Virginia).

31. W. J. Metcalf and R. L. Walker, *Nucl. Phys.* **B76**, 253 (1974).

32. N. Isgur, G. Karl and R. Koniuk, *Phys. Rev.* **D25**, 2394 (1982).

33. J. Dey and M. Dey, *Phys. Lett.* **138B**, 200 (1984).

34. R. Davidson, N. Mukhopadhyay and R. Wittman, *Phys. Rev. Lett.* **56**, 804 (1986).

35. D. Drechsel and M. M. Giannini, *Phys. Lett.* **143B**, 329 (1984).

36. M. Bourdeau and N. C. Mukhopadhyay Proc. 1986 CEBAF Summer Workshop, 135 (1986) (eds. V. Burkert *et al.*).

37. J. L. Friar and W. C. Haxton, *Phys. Rev.* **C31**, 2027 (1985).

38. V. Burkert, Proc. 1986 CEBAF Summer Workshop, 161 (1986).

39. R. P. Feynman, Lecture on the Quark Model, 1969 (unpublished)

40. M. H. Han and Y. Nambu, *Phys. Rev.* **139B**, 1006 (1965).

41. For details, see F. E. Close, "An Introduction to Quarks and Partons", Academic Press, N.Y. (1979).

42. F. Gürsey and L. A. Radicati, *Phys. Rev. Lett.* **13**, 173 (1964);
A. Pais, ibid, 175.

43. R. H. Dalitz, (1967) reprinted in Selected Lectures of Hawaii Topical Conf., Vol. 1 (eds. S. Pakvasa and S. F. Tuan, World Scientific, Singapore, 1982).

44. D. Faiman and A. W. Hendry, *Phys. Rev.* **173**, 1720 (1968).

45. A. De-Rujula, H. Georgi and S. L. Glashow, *Phys. Rev.* **D12**, 147 (1975).

46. N. Isgur and G. Karl, *Phys. Rev.* **D18**, 4187 (1978), **D19**, 2653 (1979);
C. P. Forsyth and R. E. Cutkosky, *Z. Phys.* **C18**, 219 (1983).

47. S. Capstick and N. Isgur, *Phys. Rev.* **D34**, 2809 (1986).

48. N. Isgur, G. Karl and R. Koniuk, *Phys. Rev. Lett.* **41**, 1269 (1978).

49. M. Brack and R. K. Bhaduri, *Phys. Rev.* **D35**, 3451 (1987).

50. J. J. Sakurai, "Advanced Quantum Mechanics", Addison-Wesley, Reading MA, (1967) p. 36.

51. R. G. Moorhouse, *Phys. Rev. Lett.* **16**, 772 (1966).

52. B. Silvestre-Brac and C. Gignoux, *Phys. Rev.* **D32**, 743 (1985).

53. M. V. N. Murt
D30, 152 (1
M. V. N. M

54. R. K. Bhaduri,
1369 (1980).

55. D. Gromes, *Z. I*
L. J. Reinders, i
Press, (1980).
M. V. N. Murth
Phys. **C29**, 385

53. M. V. N. Murthy, M. Dey, J. Dey and R. K. Bhaduri, *Phys. Rev.* **D30**, 152 (1984).

M. V. N. Murthy and R. K. Bhaduri, *Phys. Rev. Lett.* **54**, 745 (1985).

54. R. K. Bhaduri, L. E. Cohler and Y. Nogami, *Phys. Rev. Lett.* **44**, 1369 (1980).

55. D. Gromes, *Z. Phys.* **C18**, 249 (1983);

L. J. Reinders, in Baryon 1980, Ed. N. Isgur, p. 203, Univ. Toronto Press, (1980).

M. V. N. Murthy, M. Brack, R. K. Bhaduri and B. K. Jennings, *Z. Phys.* **C29**, 385 (1985).